Ocean Engineering 313 (2024) 119429

Contents lists available at ScienceDirect

Ocean Engineering

journal homepage: www.elsevier.com/locate/oceaneng

Research paper

Offshore floating platform synergizing internally-installed self-reacting wave energy converters for optimizing vibration control and energy harvesting

Zhicong Huang [a], Yongxing Zhang [a], Jing Bian [b,*]

[a] Shien-Ming Wu School of Intelligent Engineering, South China University of Technology, Guangzhou, 511442, China
[b] School of Civil Engineering, Chongqing University, Chongqing, 400044, China

ARTICLE INFO

Keywords:
Offshore floating platform
Wave energy converter
Self-reaction mechanism
Energy harvesting
Vibration control
Synergizing

ABSTRACT

Vibration control is essential for ensuring the safe operation of offshore floating platforms (OFPs). Although a basic combination of the OFP with wave energy converters (WECs) can realize vibration control and energy harvesting, there remains a challenge in achieving effective vibration control across a broad frequency band while facilitating efficient energy harvesting. To bridge this research gap, this paper extends the operation mechanism of internally installed WECs into the OFP vibration control scenario. This concept achieves physical isolation of the WECs from ocean waves, enabling WECs to directly absorb vibration energy from OFP and suppress its meanwhile. For illustration purposes, a semi-submersible floating platform (SSP) synergizing multiple internally-installed self-reacting WECs (SSP-SRWEC) is designed. A dynamic model is established and validated in both time and frequency domains. Based on this, dual-objective synergized optimization is conducted to determine the optimal parameters of SSP-SRWEC for both vibration control and energy harvesting purposes. Comparative analysis with a typical SSP combined with WEC demonstrates that the proposed SSP-SRWEC has the following advantages: (i) significantly enhanced vibration control over a wider frequency range, and (ii) greater energy harvesting performance under the same device conditions.

Nomenclature

Abbreviations			
OFP	Offshore floating platform	SSP-CWEC	SSP combined with wave energy converter
WEC	Wave energy converter	MSL	Mean sea level
SSP	Semi-submersible floating platform	COG	Center of mass
SRWEC	Self-reacting WEC	PTO	Power take-off
SSP-SRWEC	SSP synergy multiple internally-installed self-reacting WECs	RAO	Response amplitude operator
		OWC	Oscillating water column
Symbols			
m_p	The physical mass of SSP	$c_{wi}(i = 1,2,3)$	Damping coefficients of each SRWEC
ω	Wave frequency	z_p	Heave motion of SSP
H	Wave height	$z_{wi}(i = 1,2,3)$	Heave motion of each SRWEC
m_w	The physical mass of SRWEC	μ	Mass ratio between each SRWEC and SSP

(*continued on next column*)

(*continued*)

k_p	hydrostatic stiffness of SSP	Ω	Excitation frequency
c_p	Radiation damping of SSP	$\gamma_i(i = 1,2,3)$	Natural frequency ratio between each SRWEC and SSP
f_e	Wave excitation force	$\xi_i(i = 1,2,3)$	Damping ratio of each SRWEC
$m_{add,\infty}$	Added mass of SSP	G	Heave vibration amplitude of SSP
k_{wi} (i = 1,2,3)	Stiffness coefficients of each SRWEC	$L_i(i = 1,2,3)$	Safe motion excursion for each SRWEC

1. Introduction

The ocean has abundant renewable and non-renewable resources (Oliveira-Pinto et al., 2019; Pata, 2021; Zhao et al., 2024). Historically, energy extraction predominantly occurred in shallow water depths. However, as shallow water resources deplete and technological

* Corresponding author.
E-mail addresses: zhiconghuang@scut.edu.cn (Z. Huang), wicmyazzhangyx@mail.scut.edu.cn (Y. Zhang), bian.jing@cqu.edu.cn (J. Bian).

https://doi.org/10.1016/j.oceaneng.2024.119429
Received 11 June 2024; Received in revised form 9 September 2024; Accepted 2 October 2024
Available online 9 October 2024
0029-8018/

advancements emerge, offshore energy extraction is progressively shifting towards deeper waters (Rehman et al., 2023; Sharma et al., 2010). Offshore floating platforms (OFPs) play a pivotal role as essential infrastructure for exploring and exploiting ocean resources in deeper seas. These platforms are capable of accommodating various installations such as wind turbines, oil and gas drilling facilities, substations, wave energy converters (WECs) and so on. They fulfill the escalating energy demands accompanying rapid development and consequently attract considerable attention from numerous coastal countries (Saeed et al., 2024; Lamas-Pardo et al., 2015).

The OFP can typically be categorized into three main types: the semi-submersible floating platform (SSP) (Sharma et al., 2010), spar floating platform (Saeed et al., 2024), and tension leg floating platform (Lamas-Pardo et al., 2015). Among these, the SSP stands out due to its wide applicable water depth, expansive deck area, and substantial payload capacity, rendering it extensively utilized in engineering practice (Huang et al., 2019; Liu et al., 2016; Shi et al., 2024). However, the SSP is prone to significant heave motion under wave excitation (Emami and Gharabaghi, 2020; Halkyard, 2005) due to its small water plane, draft, and limited hydrodynamic damping. Additionally, the fundamental natural period of a SSP in the heave direction is generally close to the wave dominant period, and a large heave motion is therefore expected during its service life because of resonances (Ma et al., 2020). This excessive heave motion not only compromises the performance and comfort of crew members but also poses fatigue concerns for structural components, potentially leading to platform sinking. Therefore, mitigating the vibration response of the SSP in the heave direction is imperative to safeguard equipment and ensure the safety of operational activities.

Efforts to mitigate the heave motion of SSP have focused on three main avenues: increasing stiffness (Kandasamy et al., 2016; Ma et al., 2023), enhancing structural vibration control (Hemmati et al., 2019; Yang et al., 2019; Zhang et al., 2017), and employing wave energy converters (WECs) (Nguyen and Wang, 2020a, 2020b; Rony and Karmakar, 2022). Increasing stiffness represents a straightforward approach, shifting the resonance frequency of the SSP outside the excitation frequency band by increasing the platform's stiffness. However, this method leads to an increase in construction cost and changes the design of the existing SSP platforms, which is further making the construction more difficult. To addressing this concern, Reference (Yao, 1972) introduced the concept of structural vibration control to diminish undesirable platform vibrations. Structural vibration control involves three methods: passive, active, and semi-active (Chai et al., 2024; Farahpour and Hejazi, 2023; Huang and Yang, 2023). While semi-active and active control methods provide feedback control forces, yielding excellent vibration control performance, they necessitate additional energy inputs and maintenance-intensive mechatronic equipment. In contrast, passive vibration control methods offer stability and cost-effectiveness, mitigating the drawbacks associated with semi-active and active control approaches. Nowadays, passive control methods, such as dampers (Ma et al., 2019, 2021), isolation platforms/isolators (Bian et al., 2023; Ke et al., 2023; Ma et al., 2020), and dynamic vibration absorbers (Bian and Jing, 2020; Su et al., 2023, 2024), have been reported to mitigate the heave motion response of the platform (primary structure) to some extent. However, these reported vibration control devices are all energy-dissipation systems, meaning that the wave energy absorbed by the SSP under ocean wave excitation is dissipated and wasted. On the other hand, the offshore SSP usually necessitates significant energy inputs for operating equipment, supporting living facilities, and powering scientific research equipment. Therefore, it is desired to convert the wave energy absorbed by the SSP into useful energy, such as electric energy, for suppressing the platform vibration while providing energy for SSP operation.

To simultaneously optimize vibration control and energy harvesting, the SSP combined with wave energy converter (SSP-CWEC) has been developed (Cheng et al., 2022a, 2022b, 2024; Ghafari et al., 2021; Hu et al., 2020). The design concept behind the SSP-CWEC involves deploying multiple WECs outside the platform to absorb wave energy acting on the SSP, thereby suppressing vibrations. Initial experimental tests, as documented in some references (Gaspar et al., 2018; Kamarlouei et al., 2020; Zhu and Hu, 2016), demonstrate that deploying a WEC array around the SSP contributes to reducing platform heave motion. However, these studies only conducted time-domain analysis under fixed wave frequencies, missing the dynamic interaction between the SSP and WEC under varying wave frequencies. Through subsequent analysis in references (Tian et al., 2023; H. Zhang et al., 2023; Z. Zhang et al., 2023; Zhou et al., 2023), it can be found that the heave motion reduction of the platform only occurs within a specific wave frequency band. As wave frequencies change, the platform's vibration amplitude may even increase due to the interaction between the WEC and SSP with the ocean waves. Ocean waves incur added mass, hydrostatic stiffness, and radiation-damping effects on both the WEC and SSP, leading to the natural frequencies varying with change of wave frequencies. When the natural frequencies of the two structures are similar, the SSP's vibration amplitude increases sharply. While certain improvements have been made to the SSP-CWEC structure, such as adjustments in WEC array configuration (Gaspar et al., 2021; Kamarlouei et al., 2020), WEC shape (Wang et al., 2022; Wu et al., 2024), and the number of WECs (Ghafari et al., 2021; Hu et al., 2020; Tian et al., 2023), These methods cannot thoroughly eliminate the inherent hydrodynamic effects of ocean waves acting on the WEC. It is noteworthy that some scholars have recently proposed combining oscillating water columns (OWCs) with SSP to reduce platform vibration amplitude (Sebastian et al., 2024; Zhang et al., 2022). However, the OWCs must interact with the ocean waves to achieve energy conversion. Therefore, similar to the aforementioned research gap, the vibration control effectiveness of the combined OWC and SSP structure is still limited. In consequence, the existing SSP-CWEC structure cannot effectively reduce SSP vibration amplitude by directly absorbing platform vibration energy. Moreover, all WECs in the array share identical stiffness and damping parameters, leading to a uniform natural frequency band. Despite efforts in structural parameter optimization, the SSP-CWEC structure struggles to achieve vibration control across a border frequency band. Notably, to harvest more wave energy by maximizing motion, some WEC control or WEC farm control methods (Esmaeilzadeh and Alam, 2019; Rodríguez et al., 2020; Shadman et al., 2018) continuously tune each WEC's natural frequencies or phase to match the changing external wave conditions. However, offshore floating platforms should avoid resonance and maintain stability by minimizing motions (Emami and Gharabaghi, 2020; Sykes et al., 2023). This implies that these methods are not suitable for achieving effective vibration control for the offshore floating platform.

Building on our earlier work (Bian, 2021; Bian and Jing, 2021) in structural vibration control, we demonstrated that the effectiveness of vibration suppression in the primary structure (equivalent to the floating platform) deteriorates significantly when the damping and stiffness of the vibration absorber (equivalent to the WEC) change (i.e., parameters detuned). Given that ocean waves inevitably induce hydrostatic stiffness and radiation-damping effects on the externally deployed WEC, this paper extends the operation mechanism of internally installed WECs into floating platform vibration control. By physically isolating the WEC from ocean waves, we prevent changes in its damping and stiffness, laying the groundwork for more effective vibration control of the floating platform. It is noteworthy that some scholars have proposed some enclosing structure such as ISWEC, PEWEC, Penguin, SWINGO, etc. These devices enclose the WEC inside the hull, avoiding contact with seawater, which increases the device's durability (Khedkar et al., 2021; Pozzi et al., 2018). Moreover, to harvest more wave energy, the PTO's coefficients (stiffness and damping) are regulated to match the changing external wave frequency (Bracco et al., 2020; Carapellese et al., 2022a, 2022b). However, these works do not explore suppressing floating platform vibration or conducting vibration control-oriented numerical optimization.

To be specific, as depicted in Fig. 1, the vibrations induced in the SSP by ocean waves can be directly harvested by three self-reacting wave energy converters (SRWECs) to generate electrical energy. Simultaneously, the resultant reaction forces from these SRWECs can suppress platform vibrations. To assess the performance of the proposed SSP-SRWEC, its dynamic model is established, and the optimization of multiple SRWEC structure parameters is conducted to synergize vibration control and energy harvesting. Finally, a comparison of the proposed SSP-SRWEC with typical SSP-CWEC and SSP configurations without WECs is conducted in both time domain and frequency domain. The contributions of this study are summarized as follows:

(1) Extending the operation mechanism of internally installed WECs into the floating platform vibration control scenario and providing a numerical optimization investigation.
(2) Establishment and analysis of the dynamic model of the proposed SSP-SRWEC in both time and frequency domains. The accuracy of the dynamic model is verified through integration with ANSYS-AQWA and Simulink-SimMechanics.
(3) Development of a dual-objective optimization framework for vibration control and energy harvesting, resulting in the determination of optimal structural parameters. These findings provide valuable insights for the design of structural parameters.

The rest of this paper is organized as follows: Section 2 displays on the detailed mechanical structure design and operational principles of SSP-SRWEC. In Section 3, the equations of motion and analytical response in the frequency domain for the SSP-SRWEC are derived. Furthermore, the model's validity is confirmed through joint simulation experiments using ANSYS-AQWA and Simulink-Sim Mechanics. Section 4 conducts parameter optimization analyses in both vibration control and energy harvesting aspects, offering corresponding design guidance. Section 5 compares the performance of the proposed SSP-SRWEC with a typical SSP-CWEC in terms of vibration control and energy harvesting. Finally, Section 6 presents the conclusions drawn from this study.

2. Mechanical design and system description

Fig. 2(a) illustrates a schematic diagram of a SSP-SRWEC, comprising three SRWECs and a SSP. The three SRWECs, designated as SRWEC-1, SRWEC-2, and SRWEC-3, are internally installed on the side columns of the SSP. As waves propagate through the SSP-SRWEC, the SSP undergoes oscillations in the heave direction, prompting the internal SRWECs to move and generate electricity. Simultaneously, the resultant reaction forces from these SRWECs can suppress platform vibrations. Throughout this process, the vibration energy of the SSP induced by the waves is directly absorbed by the three SRWECs, effectively achieving the objectives of vibration control and energy harvesting.

As shown in Fig. 2(b), the SRWEC mainly includes two parts: oscillating body and power take-off (PTO). Among them, the oscillating body converts the vibration energy of SSP into the oscillating body's mechanical energy and transmits it to the PTO system. Moreover, in order to ensure the continuity and stability of power generation, the PTO is designed as a self-rectifying type (Falcão et al., 2018; Yang et al., 2021; Yin et al., 2019) by utilizing the one-way rotation characteristic of the one-way bearing. That is the output current direction of the PTO remains unchanged no matter how the oscillating body moves. The specific mechanical transmission process can be referred to in our previous work (Y. Zhang et al., 2023), and will not be repeated here.

The geometric structural relationship of the SSP-SRWEC concept is illustrated in Fig. 3. The platform is located in waters with a water depth of 300 m and a draft of 31.5 m, utilizing mooring lines for station-keeping. The global coordinate system O is positioned at the initial position of the platform and on the mean sea level (MSL). The overall structure is axially symmetrical, with a horizontal distance l_{cs} between the center point of each SRWEC and the SSP center of mass (COG) is equal to 28.87 m. Additionally, the radius of the three side columns equals 11.88 m. The detailed structure parameters are listed in Table 1.

3. Modeling and validation

To effectively analyze the performance in vibration control and energy harvesting of the proposed SSP-SRWEC, this section establishes its motion equation and frequency domain analytical response based on linear potential theory (Bao et al., 2023; Tao et al., 2021), and determines the motion response of the SSP and SRWEC under regular waves. Finally, the simulation model of SSP-SRWEC is established in ANSYS-AQWA and Simulink-SimMechanics, which is used to verify the accuracy of the theoretical modeling obtained.

3.1. Equations of motion

As shown in Fig. 4, the SSP has the mass of $m_p + m_{add}(\omega)$, where the m_p represents the physical mass of the SSP, and the $m_{add}(\omega)$ denotes the

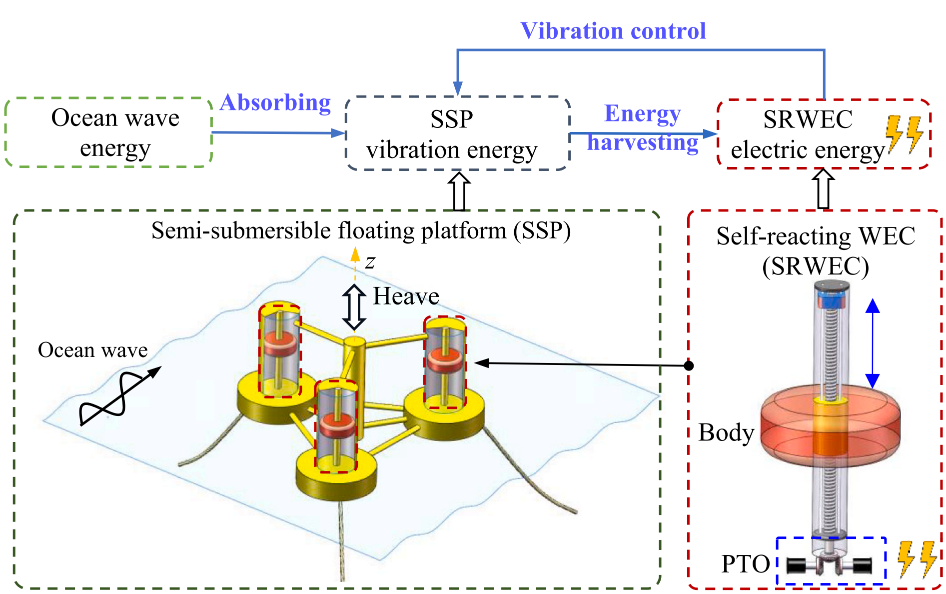

Fig. 1. Design conception of the semi-submersible platform synergy WEC with self-reaction mechanism.

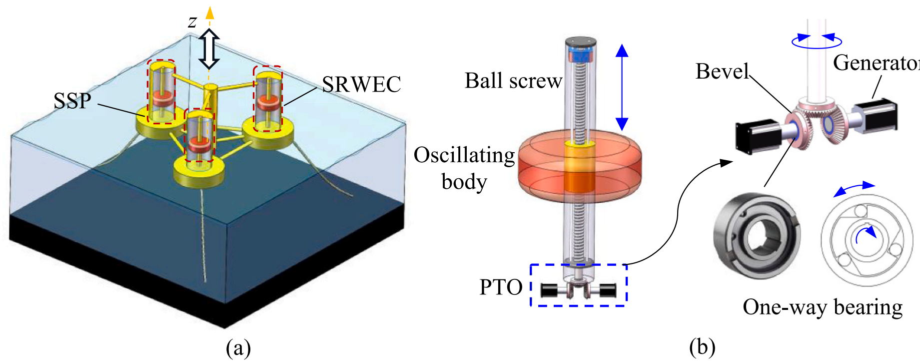

Fig. 2. Mechanical structure of the SSP-SRWEC: (a) overall structure schematic diagram, (b) self-reacting wave energy converter.

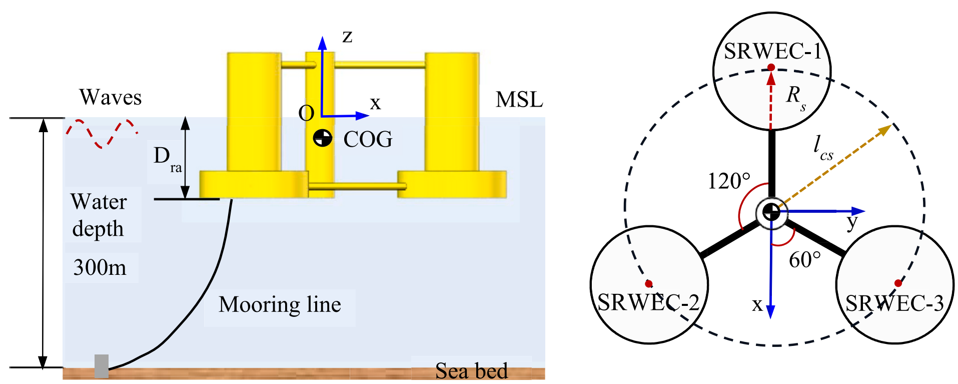

Fig. 3. Geometric structural relationship of the proposed SSP-SRWEC.

Table 1
Detailed structure parameters of the SSP-SRWEC.

Configuration	Item	Symbol	Value
SSP	Distance from the central column to the three side columns	l_{cs}	28.87 m
	Radius of the central column	R_c	6.44 m
	Radius of the three side columns	R_s	11.88 m
	Operating draft	D_{ra}	31.5 m
	Center of mass	COG	(0,0, −2.5 m)
	Mass	m_p	1500 t
	Mass moment of inertia about X axis	I_{xx}	7.53*10^8 kg*m^2
	Mass moment of inertia about Y axis	I_{yy}	7.53*10^8 kg*m^2
	Mass moment of inertia about Z axis	I_{zz}	1.22*10^9 kg*m^2
	Water depth	D_p	300 m
SRWEC	Mass	m_w	105 t
	Diameter of the central column	R_c	5 m
	Mass moment of inertia about X axis	I_{xx}	1.22*10^6 kg*m^2
	Mass moment of inertia about Y axis	I_{yy}	1.22*10^6 kg*m^2
	Mass moment of inertia about Z axis	I_{zz}	2.07*10^6 kg*m^2

frequency-dependent added mass, which is because the vibrating floating platform can drive the surrounding seawater and thereby generate an inertial force on the platform. In addition, the three SRWECs, each with a mass of m_w, are connected to the SSP through three PTOs. Notably, in engineering practice, the PTO includes viscous effects and other mechanical/electrical losses, which can cause performance loss in the electrical energy converted by the WEC (Rodríguez et al., 2019; Vervaet et al., 2022). However, these performance loss factors simply imply that a portion of the absorbed vibration energy by the SRWECs is dissipated instead of being converted into electrical energy. Nevertheless, it does not affect the core objective of vibration control in this paper. Moreover, it is challenging to quantify performance loss for the proposed SSP-SRWEC in the conceptual design stage without bench tests and practical experiments for characterization. Therefore, we utilize the widely-accepted spring-damping systems to represent the PTO, which simplifies the analysis and provides a reasonable estimation of system behavior in the absence of detailed empirical data (Hu et al., 2020; Muliawan et al., 2013; Ropero-Giralda et al., 2021). The stiffness and damping coefficients are set as k_{w1}, c_{w1}, k_{w2}, c_{w2}, k_{w3} and c_{w3}, respectively.

The SSP is connected to the reference base via hydrostatic stiffness k_p and a damper $c_p(\omega)$ (where $c_p(\omega)$ represents the frequency-dependent radiation damping), and excited by the wave excitation force f_e. Notably, the reference base is not an actual physical foundation, and it symbolizes the support offered by seawater. A detailed explanation of the above parameters will be presented subsequently.

The equation of motion can be conducted by utilizing the Lagrange equation. The kinetic energy T, potential energy V and dissipated energy D of SSP-SRWECs can be obtained as follows:

$$T = \left(m_p + m_{add,\infty}\right)\frac{\dot{z}_p^2}{2} + m_w\frac{\dot{z}_{w1}^2 + \dot{z}_{w2}^2 + \dot{z}_{w3}^2}{2} \tag{1}$$

$$V = \frac{k_p z_p^2}{2} + \frac{k_{w1}\left(z_{w1} - z_p\right)^2 + k_{w2}\left(z_{w2} - z_p\right)^2 + k_{w3}\left(z_{w3} - z_p\right)^2}{2} \tag{2}$$

$$D = \frac{c_{w1}\left(\dot{z}_{w1} - \dot{z}_p\right)^2 + c_{w2}\left(\dot{z}_{w2} - \dot{z}_p\right)^2 + c_{w3}\left(\dot{z}_{w3} - \dot{z}_p\right)^2}{2} \tag{3}$$

where the $m_{add,\infty}$ is the infinite-frequency added mass of the SSP in the heave direction, z_p is the motion displacement of SSP, z_{w1}, z_{w2} and z_{w3} are represent the motion displacement of the three SRWECs,

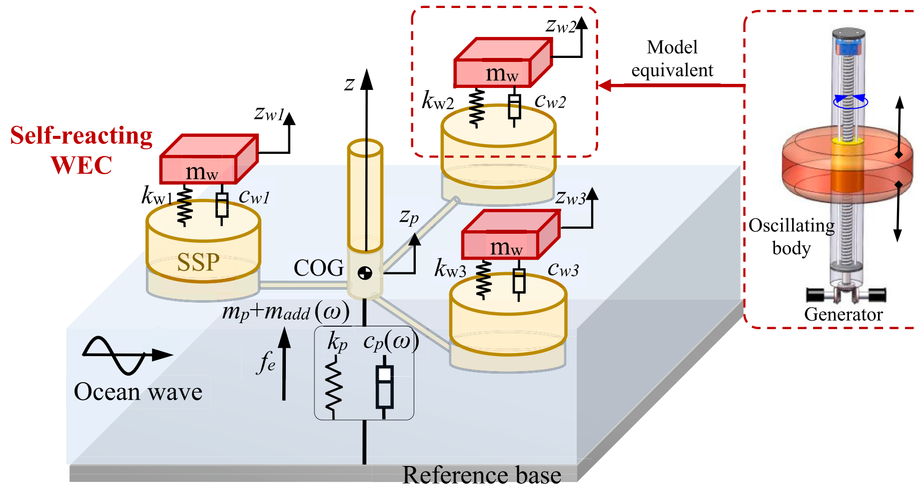

Fig. 4. Dynamic model of the SSP-SRWEC.

respectively. $\dot{z}_{w1}$, $\dot{z}_{w2}$ and $\dot{z}_{w3}$ are denote the velocity of the three SRWECs, respectively.

The general Lagrange principle is given by

$$\frac{d}{dt}\left(\frac{\partial T}{\partial \dot{z}}\right)-\frac{\partial T}{\partial z}+\frac{\partial V}{\partial z}+\frac{\partial D}{\partial \dot{z}}=f \tag{4}$$

According the general Lagrange principle in Eq. (4), the equations of motion for the SSP-SRWECs system can be obtained

$$(m_p+m_{add,\infty})\ddot{z}_p+\left(k_p+\sum_{i=1}^{3}k_{wi}\right)z_p-\sum_{i=1}^{3}k_{wi}z_{wi}+\sum_{i=1}^{3}c_{wi}\dot{z}_p-\sum_{i=1}^{3}c_{wi}\dot{z}_{wi}=f_e(t)-f_{rad}(t) \tag{5a}$$

$$m_w\ddot{z}_{wi}+k_{wi}(z_{wi}-z_p)+c_{wi}(\dot{z}_{wi}-\dot{z}_p)=0 \quad i=1,2,3 \tag{5b}$$

where, $f_e(t)$ is the wave excitation forces. Under regular wave conditions, the wave excitation force in time-domain is given by $f_e(t) = 0.5H|f_{RAO}(j\omega_n)|\cos(\omega_n t+\zeta_n+\theta_n)$. While under the irregular wave conditions, it can be expressed as $f_e(t) = \sum_{n=1}^{N}\sqrt{2S(\omega_n)\Delta\omega}|f_{RAO}(j\omega_n)|\cos(\omega_n t+\zeta_n+\theta_n)$. In these two formulas, $|f_{RAO}(j\omega_n)|$ is wave excitation force amplitude at wave frequency ω_n, and θ_n is the corresponding phase angle. N is the number of regular wave components, an irregular wave is considered to be a superposition of n regular waves. ω is from 0.1 rad/s to 3.14 rad/s $\Delta\omega = 0.031$ rad/s. ζ_n is the random phase angle, and $S(\omega)$ is the wave spectrum density function. The $f_{rad}(t)$ is the radiation damping term due to the change in momentum of the fluid resulting from the motions of SSP.

According to Cummins equation (Cummins, 1962), the radiation damping term $f_{rad}(t)$ can be expressed by convolution term, which represents the memory effect of the free surface.

$$f_{rad}(t)=\int_0^t K(t-\tau)\dot{z}_p(\tau)d\tau \tag{6}$$

where $K(t)$ is the retardation function used to describe the radiation damping force of the SSP in heave direction, and its expression is a convolution of radiation damping:

$$K(t)=\frac{2}{\pi}\int_0^\infty c_p(\omega)\cos(\omega t)d\omega \tag{7}$$

By performing a Fourier transform on the retardation function $K(t)$, we obtain:

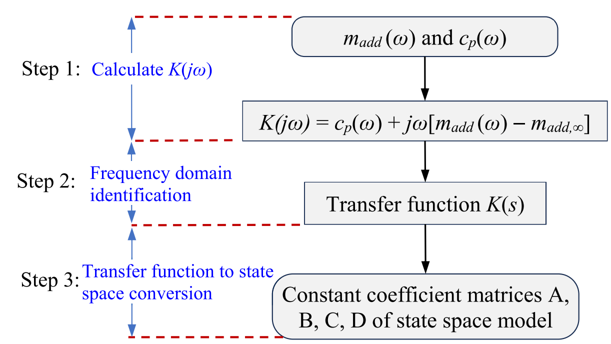

Fig. 5. The solution process of constant coefficient matrices.

$$K(j\omega)=\int_0^\infty K(t)e^{-j\omega t}dt=c_p(\omega)+j\omega[m_{add}(\omega)-m_{add,\infty}] \tag{8}$$

The retardation function $K(t)$ in convolution term $f_{rad}(t)$ essentially serves as the transfer function. Therefore, the convolution term $f_{rad}(t)$ can be regarded as a description of a linear system. Generally, its solution is approximated using the state space model substitution method (Taghipour et al., 2008).

$$\begin{cases} f_{rad}(t)=\mathrm{C}\mu(t)+\mathrm{D}\dot{z}_p(t) \\ \dot{\mu}(t)=\mathrm{A}\mu(t)+\mathrm{B}\dot{z}_p(t) \end{cases} \tag{9}$$

where $\mu(t)$ denotes the state variables of the state space model, and A, B, C and D are constant coefficient matrices that describe the model. Fig. 5 provides the specific steps for solving the above constant coefficient matrices.

Step1: Calculate the frequency domain response $K(j\omega)$ of the convolution term using the frequency-dependent added mass m_{add} (ω), frequency-dependent radiation damping $c_p(\omega)$, and Eq. (8).
Step2: Use the frequency domain regression method to identify the model and obtain the transfer function $K(s)$. Here, the nonlinear least square method is used for frequency domain identification.
Step3: Finally, use tf2ss to convert the transfer function into a state space model description and obtain the constant coefficient matrices.

According to the above solution process, the constant coefficient matrices A, B, C and D can be expressed as follows:

$$A=\begin{bmatrix}-6.46\times10^{6} & -4.41\times10^{3} & -178.78 & -18.65 & -5.36 & -2.29\\ 4096 & 0 & 0 & 0 & 0 & 0\\ 0 & 256 & 0 & 0 & 0 & 0\\ 0 & 0 & 16 & 0 & 0 & 0\\ 0 & 0 & 0 & 4 & 0 & 0\\ 0 & 0 & 0 & 0 & 2 & 0\end{bmatrix} \tag{10}$$

$$B=\begin{bmatrix}4194304 & \mathbf{0}_{1\times5}\end{bmatrix}^{T}, C=\begin{bmatrix}4.62\times10^{6} & 2799.12 & 117.83 & 10.09 & 0.42 & 0\end{bmatrix}, D=0$$

Fig. 6 compares the results of the retardation function $K(t)$ obtained from the state-space model and the hydrodynamic software ANSYS AQWA. Both display a good agreement. Thus, the state space model derived from Eqs. (9) and (10) can effectively simulate the radiation damping term $f_{rad}(t)$ in the time domain.

By expressing Eq. (5a) and Eq. (5b) in matrix form, and then substituting Eq. (9) into it, we can obtain the following

$$\begin{cases}\boldsymbol{M}\ddot{\boldsymbol{z}}(t)+\boldsymbol{C}\dot{\boldsymbol{z}}(t)+\boldsymbol{K}\boldsymbol{z}(t)=\begin{bmatrix}f_e(t)-C\mu(t)-D\dot{z}_p(t) & \mathbf{0}_{1\times3}\end{bmatrix}^{T}\\ \dot{\mu}(t)=A\mu(t)+B\dot{z}_p(t)\end{cases} \tag{11}$$

where the $\boldsymbol{z}(t)=\begin{bmatrix}z_p(t) & z_{w1}(t) & z_{w2}(t) & z_{w3}(t)\end{bmatrix}^{T}$ is the motion displacement vector in the time domain, $\dot{\boldsymbol{z}}(t)$ and $\ddot{\boldsymbol{z}}(t)$ are the corresponding velocity and acceleration vectors in the time domain. $\boldsymbol{M}$, $\boldsymbol{C}$ and $\boldsymbol{K}$ can be expressed as

$$\boldsymbol{M}=\begin{bmatrix}m_p+m_{add,\infty} & 0 & 0 & 0\\ 0 & m_w & 0 & 0\\ 0 & 0 & m_w & 0\\ 0 & 0 & 0 & m_w\end{bmatrix}, \boldsymbol{C}=\begin{bmatrix}c_{w1}+c_{w2}+c_{w3} & -c_{w1} & -c_{w2} & -c_{w3}\\ -c_{w1} & c_{w1} & 0 & 0\\ -c_{w2} & 0 & c_{w2} & 0\\ -c_{w3} & 0 & 0 & c_{w3}\end{bmatrix}$$
$$\boldsymbol{K}=\begin{bmatrix}k_p+k_{w1}+k_{w2}+k_{w3} & -k_{w1} & -k_{w2} & -k_{w3}\\ -k_{w1} & k_{w1} & 0 & 0\\ -k_{w2} & 0 & k_{w2} & 0\\ -k_{w3} & 0 & 0 & k_{w3}\end{bmatrix} \tag{12}$$

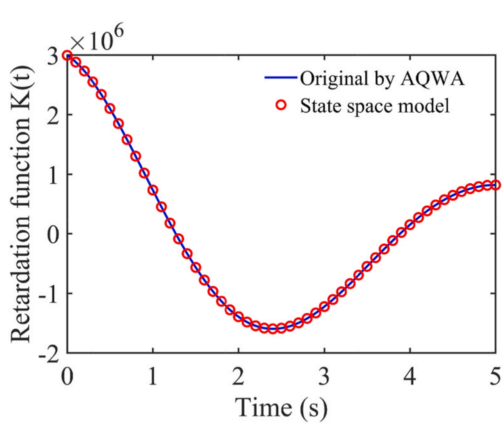

Fig. 6. The identification results comparison of retardation function $K(t)$.

Using the typical Runge-Kutta method (Blum, 1962), the second-order differential equation set Eq. (11) is solved, yielding the motion displacement in the heave direction of the floating platform and three SRWECs, and are denoted as z_p, z_{w1}, z_{w2} and z_{w3}, respectively.

3.2. Analytical response in frequency domain

To derive the frequency-domain analytical response of the SSP-SRWEC, by performing Fourier transform on Eq. (5a) and Eq. (5b), the system's motion response model in the frequency domain can be obtained as follows:

$$-\omega^2\left[m_p+m_{add}(\omega)\right]Z_p(j\omega)=\left[-k_p-j\omega c_p(\omega)\right]Z_p(j\omega)+\sum_{i=1}^{3}\left\{(k_{wi}+j\omega c_{wi})\left[Z_{wi}(j\omega)-Z_p(j\omega)\right]\right\}+F_e(j\omega) \tag{13}$$

$$-\omega^2 m_w Z_{wi}(j\omega)=-k_{wi}\left[Z_{wi}(j\omega)-Z_p(j\omega)\right]-j\omega c_{wi}\left[Z_{wi}(j\omega)-Z_p(j\omega)\right] \quad i=1,2,3 \tag{14}$$

where the $F_e(j\omega)$, $Z_p(j\omega)$, $Z_{w1}(j\omega)$, $Z_{w2}(j\omega)$ and $Z_{w3}(j\omega)$ denote the frequency-domain representations of their respective corresponding time-domain physical quantities.

Slove the above equations

$$Z_p(j\omega)=\frac{F_e(j\omega)}{\left\{-\left[m_p+m_{add}(\omega)\right]\omega^2+k_p+j\omega c_p(\omega)\right\}-\sum_{i=1}^{3}\frac{m_w\omega^2(j\omega c_{wi}+k_{wi})}{-m_w\omega^2+j\omega c_{wi}+k_{wi}}} \tag{15}$$

$$Z_{wi}(j\omega)=\frac{(k_{wi}+j\omega c_{wi})Z_p(j\omega)}{-m_w\omega^2+j\omega c_{wi}+k_{wi}} \tag{16}$$

The SRWEC employs the relative motion between oscillating body and SSP to harvest energy, and the output power of each SRWEC can be expressed as:

$$P_{wi}=\frac{1}{2}c_{wi}\omega^2\left|Z_p(j\omega)-Z_{wi}(j\omega)\right|^2 \tag{17}$$

3.3. Model validation

To verify the modeling accuracy in Section 3.1, the SSP-SRWECs are simulated under the different regular wave conditions and compared with the numerical analysis results of the theoretical model. System structural parameters are adopted from Table 1, and the other parameters for the numerical analysis include $k_p = 3.635 \times 10^3$ kN/m, $k_{w1} = 60$ kN/m, $c_{w1} = 5$ kNs/m, $k_{w2} = 70$ kN/m, $c_{w2} = 6$ kNs/m, $k_{w3} = 80$ kN/m, and $c_{w3} = 2$ kNs/m.

The frequency-dependent coefficients such as added mass and radiation damping can be calculated based on the potential theory. Among current methods, boundary element method (BEM) based on the linear potential flow theory has provided relatively accurate results at low computational costs. Various boundary element method (BEM) based hydrodynamic codes (e.g., WAMIT, NEMOH, ANSYS AQWA) have been developed and implemented in commercial software packages (Babarit and Delhommeau, 2015; Wei et al., 2024; Zou and Abdelkhalik, 2020). Moreover, it should be noted that the fully nonlinear potential flow theory has gained substantial attention due to its ability to accurately capture the complex dynamics of fluid-structure interactions. This theory offers a more precise and robust framework for analyzing wave-structure interactions. Notable contributions from Tezdogan et al. (2016a, 2016b, 2015), Terziev et al. (2022, 2021, 2020) and Kim et al. (2021b, 2021a) have significantly advanced both the theoretical understanding and practical applications in this field. Considering accuracy and calculation cost, we have selected ANSYS AQWA commercial software to calculate these hydrodynamic parameters, which are shown in Appendix A1 for brevity.

1) Simulation model construction

The simulation of SSP-SRWEC involves the coupling of hydrodynamics and multi-body mechanical dynamics. To achieve this goal, the ANSYS-AQWA and Simulink-SimMechanics are chosen for integration in simulation. The advantage of this modeling technique is its ability to easily integrate multi-body models with other modules that define hydrostatic/hydrodynamic forces and behavior (Albert et al., 2017; Bruzzone et al., 2020). Fig. 7 shows the detailed simulation framework of the simulation model SSP-SRWEC.

The simulation system used for model verification for SSP-SRWEC includes two parts: hydrodynamics and mechanical dynamics. Specifically.

- **Hydrodynamics:** Generate the grids of the SSP using ANSYS-AQWA, and calculate hydrodynamic coefficients such as added mass, radiation damping, and wave excitation force in the frequency domain. Based on this, using mathematical software MATLAB, we calculated the wave excitation force $f_e(t)$ in the time domain, infinite-frequency added mass $m_{add,\infty}$, hydrostatic stiffness k_p and constant coefficient matrices A, B, C, and D that describe the retardation function $K(t)$ in radiation damping force.

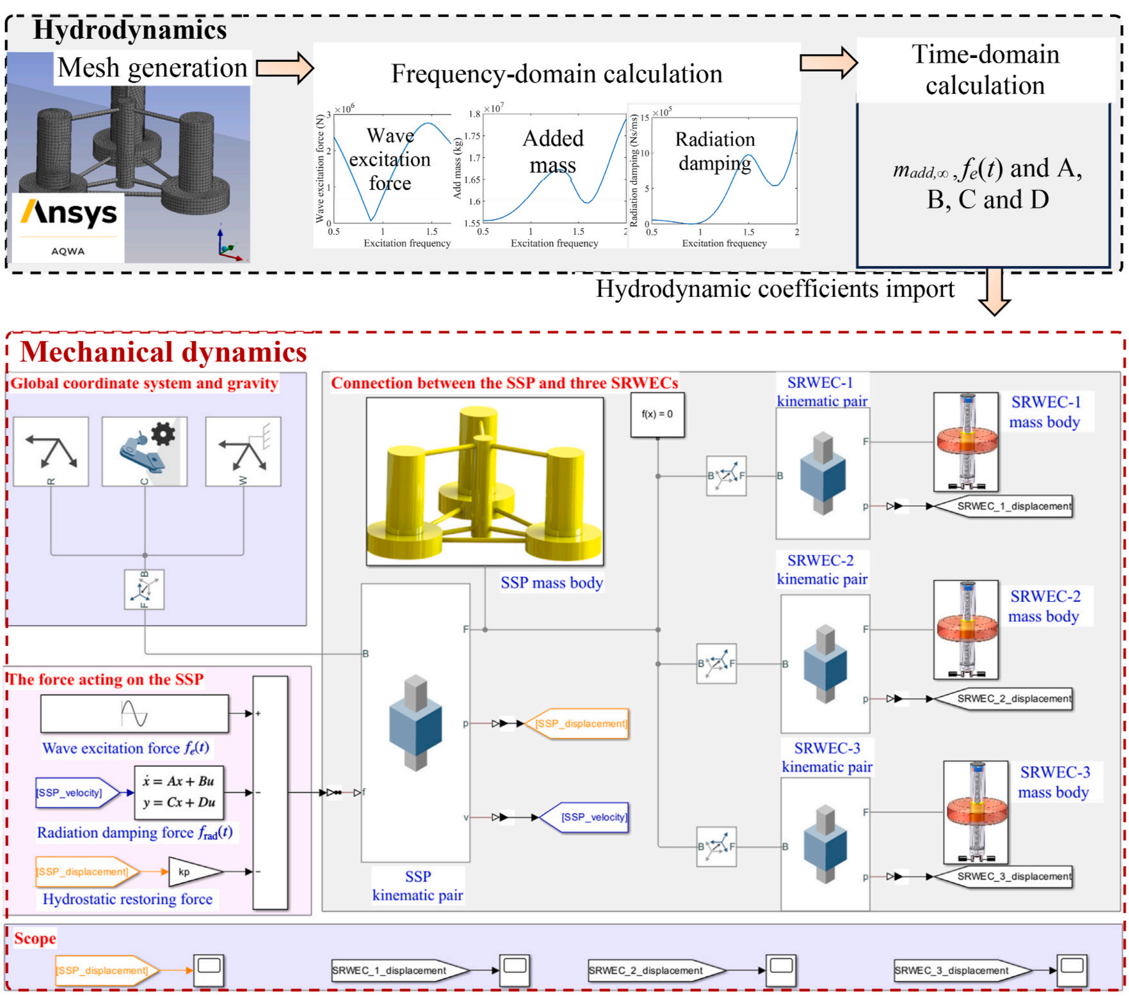

Fig. 7. Framework of the simulation model for SSP-SRWEC.

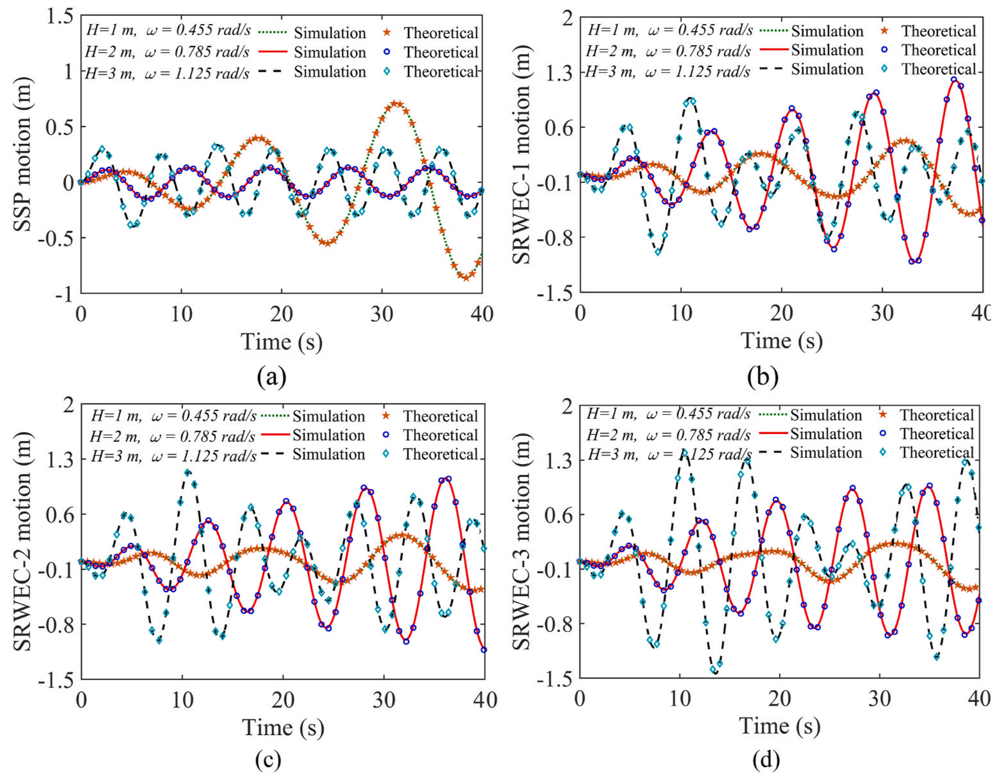

Fig. 8. Theoretical model verification under different regular wave conditions: (a) SSP motion, (b) SRWEC-1 motion, (c) SRWEC-2 motion and (d) SRWEC-3 motion.

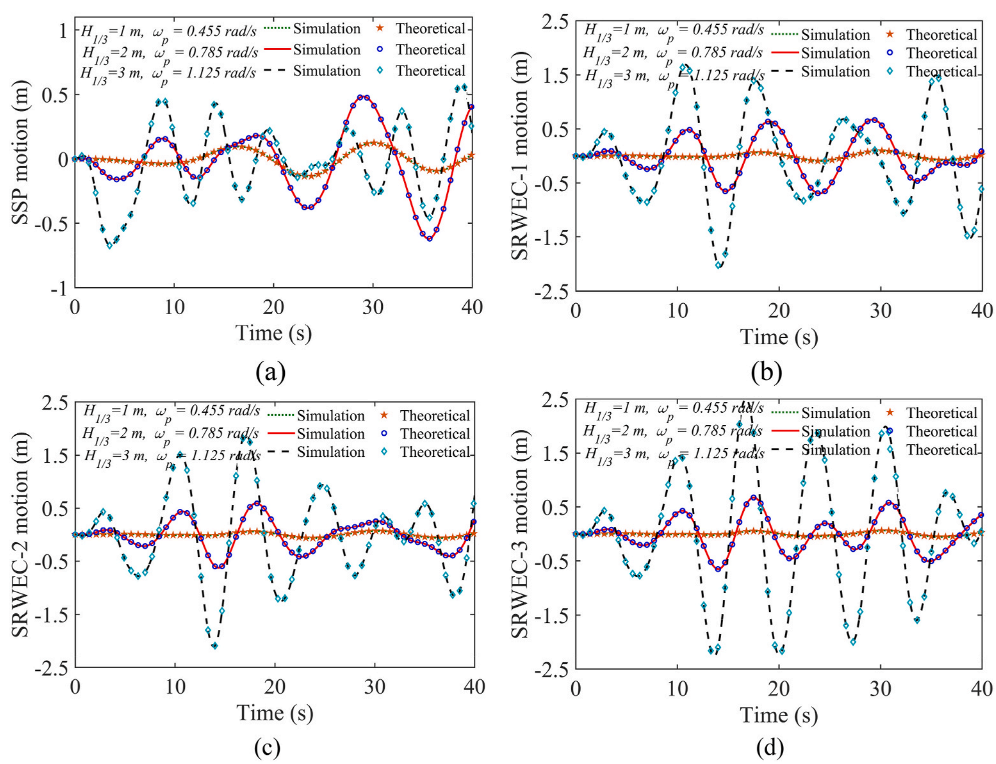

Fig. 9. Theoretical model verification under different irregular wave conditions: (a) SSP motion, (b) SRWEC-1 motion, (c) SRWEC-2 motion and (d) SRWEC-3 motion.

- **Mechanical Dynamics:** Set the global coordinate system and gravity. Then, use kinematic pairs to connect the mass bodies of the SSP and the three SRWECs based on their relative positions and motion relationships. Import the system structural parameters, the stiffness and damping coefficients of the three SRWECs, and the infinite-frequency added mass of the SSP into the corresponding mass bodies and kinematic pairs. Based on the above-calculated hydrodynamic coefficients, construct modules for the wave excitation

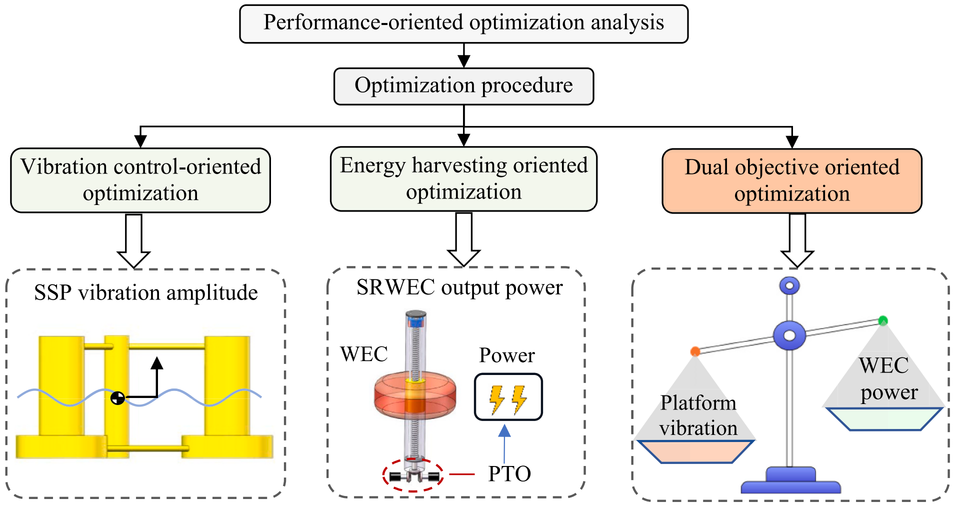

Fig. 10. Framework of performance-oriented optimization analysis of SSP-SRWEC.

force, radiation damping force, and restoring force in the time domain. Exert these forces on the kinematic pair of the SSP, and use the scope to observe the motion displacement of the SSP and the three SRWECs.

2) Model verification

Based on the above structural parameters, the heave motion of the SSP-SRWEC is obtained by the simulation analysis in Simulink. Three regular wave conditions, characterized by $H = 1$ m, $\omega = 0.455$ rad/s, $H = 2$ m, $\omega = 0.785$ rad/s, and $H = 3$ m, $\omega = 1.125$ rad/s, respectively, are considered to verify the accuracy of the model. As shown in Fig. 8, the motion displacements of the SSP and three SRWECs obtained by the theoretical analysis method (refer to Section 3.1) are in good agreement with the simulation results. This alignment demonstrates the validity of the present theoretical model and calculation program.

Without validation in regular waves, the three irregular wave conditions, characterized by significant wave heights and their corresponding peak frequencies ($H_{1/3} = 1$ m, $\omega_p = 0.455$ rad/s, $H_{1/3} = 2$ m, $\omega_p = 0.785$ rad/s, and $H_{1/3} = 3$ m, $\omega_p = 1.125$ rad/s, are also considered to verify the correctness of the model. The irregular wave spectrum density function $S(\omega) = 16.43\frac{\omega_p^4 H_{1/3}^2}{\pi^4\omega^5}\exp\left(-\frac{\omega_p^4 65.74}{\pi^4\omega^4}\right)$ is adopted, and it is based on statistical data fitting from the China National Marine Data Center ("National Science & Technology Infrastructure. Measured Data. Available at: http://mds.nmdis.org.cn) for the northern coast of the South China Sea. As shown in Fig. 9, the motion displacements of the SSP and the three SRWECs, obtained using the theoretical analysis method (refer to Section 3.1), are in close agreement with the simulation results. This consistency further confirms the validity of the present theoretical analysis and calculation program.

4. Performance-oriented optimization analysis

From a structural design perspective, the proposed SSP-SRWEC serves dual functions of vibration control and energy harvesting. In order to reveal its internal mechanism and optimal performance, as depicted in Fig. 10, we first establish the optimization procedure of the SSP-SRWEC based on the model obtained in Section 3. Next, parameter optimization is conducted separately for vibration control and energy harvesting. Subsequently, with the consideration of both vibration control and energy harvesting performances, Pareto search method is applied to the optimization objective to explore the comprehensive performance regarding the aforementioned two aspects.

4.1. Optimization procedure

An optimization task generally contains three indispensable elements: optimization objective, constraint condition and optimization method. The optimization procedure of SSP-SRWEC will be detailed from these three aspects. Moreover, to make the optimization analysis results more universal, the non-dimensional parameters used here are given below: $\mu = m_w/m_p$, $\Omega = \omega/\sqrt{k_p/(m_P + m_{add})}$, $\gamma_i = \sqrt{k_{wi}/m_w}/\sqrt{k_p/m_p}$ and $\xi_i = c_{wi}/2\sqrt{k_{wi}m_w}$. Where μ is the mass ratio between each SRWEC and SSP; Ω is the excitation frequency; γ_i is the natural frequency ratio between each SRWEC and SSP; ξ_i is the damping ratio of each SRWEC.

(a) Optimization objective

For vibration control, the optimization objective of SSP-SRWEC is to minimize the maximum amplitude of the primary structure (i.e., SSP) in the dangerous frequency range (near resonant frequency) to ensure the stability of the SSP. Thus, this is a typical minimizing the maximum optimization problem (Bian and Jing, 2021), which can be expressed as

$$J_v = \min_{\gamma_i,\xi_i}\left[\max_{\Omega_1\le\Omega\le\Omega_2} G(\gamma_i,\xi_i,\Omega)\right] \quad i = 1, 2, 3 \tag{18}$$

where G represent the vibration amplitude of the SSP in heave direction.

For energy harvesting, the pursuit of maximum energy harvesting is our main concern. In view of the uncertainty of the actual wave motion frequency, the maximum of mean power $\overline{P}$ under the excitation frequency band $[\Omega_1, \Omega_2]$ is taken as the optimization target. Following this concept, we have

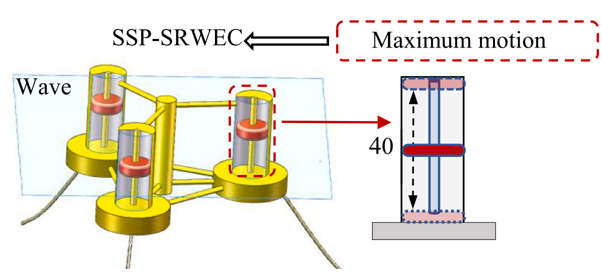

Fig. 11. The maximum motion limit of SRWEC. (c) Optimization method.

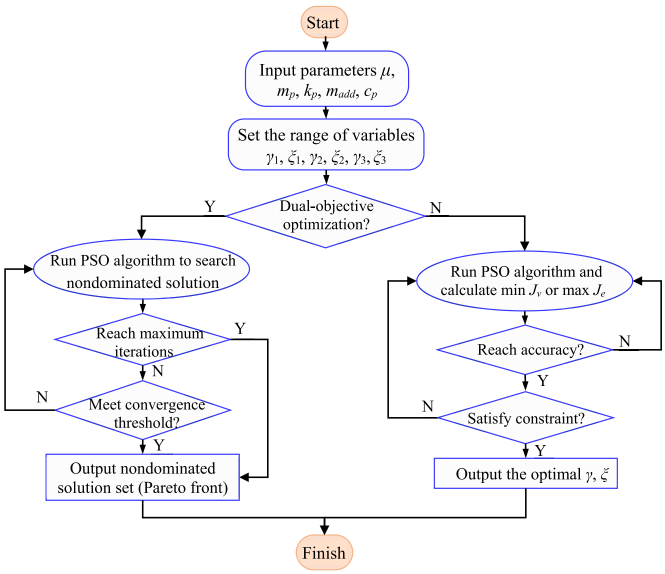

Fig. 12. Optimal parameter searching method.

$$J_e = \max_{\gamma_i,\xi_i}\left[\overline{\mathrm{P}}(\gamma_i,\xi_i,\Omega)_{\Omega_1\le\Omega\le\Omega_2}\right] \quad i=1\ ,\ 2\ ,\ 3 \tag{19}$$

For dual-objective optimization of vibration control and energy harvesting, Pareto search is used as it can reveal the entire Pareto front of solutions with rich diversity for one to examine without any prior information about the preferences (Calinescu et al., 2018; Chen et al., 2019; Zhang et al., 2018). Combining Eqs. (17) and (18), the dual objective for optimization can be written as follows:

$$J = \underset{\gamma_i,\xi_i}{\mathrm{minimizing}}\{J_v, -J_e\} \quad i=1\ ,\ 2\ ,\ 3 \tag{20}$$

where the negative of J_e is minimized, leading to the maximization of the mean power output.

(b) Constraint condition

In the optimization process, it is necessary to consider the actual physical constraints to ensure the practicality of the optimization results. As depicted in Fig. 11, due to structural constraints, the vibration amplitude of the SRWEC is limited by the operating range. Exceeding these limits will result in equipment damage. To be specific, for the SSP-SRWEC discussed in this study, the restrictions on the maximum motion displacement L_i for each SRWEC are as follows.

$$\max_{\Omega_1\le\Omega\le\Omega_2} L_i \le 40\mathrm{m} \quad i=1\ ,\ 2\ ,\ 3 \tag{21}$$

Given that the optimization objective involves six optimization variables $[\gamma_1, \xi_1, \gamma_2, \xi_2, \gamma_3, \xi_3]$, the traditional loop iteration method has disadvantages in terms of long solution time and low accuracy. As a heuristic algorithm for multi-parameter optimization, particle swarm optimization (PSO) (Marini and Walczak, 2015) has short search time and high-precision global search capabilities. Therefore, it is relatively appropriate to choose PSO for multi-variable synergized optimization work including damping ratio and frequency ratio. The optimal parameter optimization method using PSO is shown in Fig. 12.

4.2. Vibration control-oriented optimization

Before executing the optimization procedure, the system structural parameter ranges in the optimization programming are set as $\gamma_i \in (0\ ,\ 0.8)$, $\xi_i \in (0\ ,\ 0.2)$ and $\Omega \in [0.5\ ,\ 2]$. Mass ratio μ is fixed as 0.07. In order to make the results more general, the ratio of the amplitude of SSP and SRWEC to the wave amplitude is defined as their respective response amplitude operator (RAO). Employing the proposed optimization procedure in MATLAB 2022, as shown in Fig. 13(a), the optimal value of $\min_{\gamma_i,\xi_i,\Omega}(\max_{\Omega_1\le\Omega\le\Omega_2}\mathrm{G}(\gamma_i,\xi_i,\Omega))$ is 1.78. This implies that even at the most dangerous resonant frequency, the amplitude of the SSP is amplified by only a factor of 1.78. The proposed SSP-SRWEC achieves a 92.2% reduction in maximum vibration amplitude compared to the SSP without WEC at this frequency. The above results confirm the excellent vibration suppression performance of the proposed SSP-SRWEC.

It can be observed from Fig. 13(b) that, compared to the SSP's maximum amplitude of only 1.78, the three SRWECs have much larger vibration response peaks (around 17.8). Since changes in vibration amplitude reflect changes in energy, this result confirms that the vibration energy of the SSP is effectively transferred to the SRWECs in the

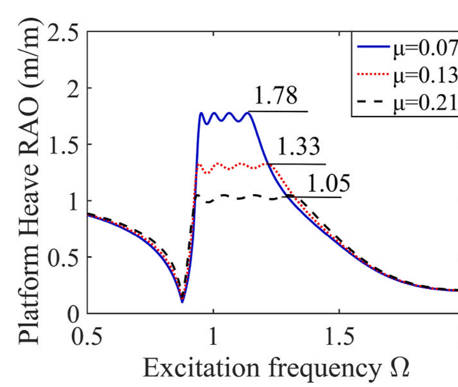

Fig. 14. The frequency-domain response amplitude operator of SSP-SRWEC in different mass ratios.

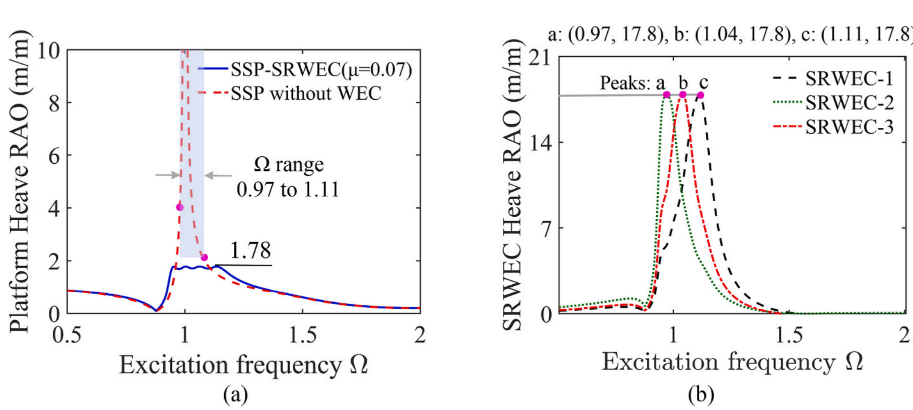

Fig. 13. The frequency-domain response amplitude operator: (a) SSP and (b) SRWEC.

Table 2
Optimal frequency ratio and damping ratio under different mass ratio for vibration control.

Mass ratio	γ_1	ξ_1	γ_2	ξ_2	γ_3	ξ_3
$\mu = 0.07$	0.2847	0.0438	0.3017	0.0438	0.3208	0.0441
$\mu = 0.09$	0.2853	0.0514	0.3042	0.0542	0.3263	0.0509
$\mu = 0.11$	0.2859	0.0564	0.3076	0.0604	0.3318	0.0593
$\mu = 0.13$	0.2863	0.0609	0.3110	0.0611	0.3382	0.0628
$\mu = 0.15$	0.2870	0.0658	0.3139	0.0660	0.3439	0.0660
$\mu = 0.17$	0.2879	0.0678	0.3178	0.0656	0.3501	0.0684
$\mu = 0.19$	0.2890	0.0723	0.3202	0.0714	0.3556	0.0690
$\mu = 0.21$	0.2897	0.0812	0.3226	0.0780	0.3591	0.0770

dangerous frequency range (near the resonant frequency). Interestingly, although the three SRWECs have the same peak values, they correspond to different excitation frequencies: 0.97 for SRWEC-1, 1.04 for SRWEC-2, and 1.11 for SRWEC-3. This is because the optimization objective of vibration control is to minimize the SSP's maximum vibration response across a wide frequency range, essentially employing robust H_∞ optimization. By optimizing in this way, SRWECs with the same vibration peak but different natural frequencies can effectively disperse vibration energy and expand the bandwidth of vibration control.

In engineering practice, the mass ratio μ may change under certain conditions (Bian et al., 2022). For example, if the SSP loses or gains weight due to different operating tasks, the mass ratio μ of the entire system changes. Therefore, it is necessary to optimize the structural parameters γ_i and ξ_i of the SRWECs under different mass ratios μ, thus maintaining the vibration control effectiveness. It is observed from Fig. 14 that as the mass ratio μ increases, the vibration amplitude of the floating platform is more efficiently suppressed with the SRWECs. This implies that if there is no limit on the mass of the SRWEC, the mass ratio μ can be designed to be large enough to suppress the amplitude of the floating platform as much as possible. However, the larger mass of SRWEC means that the investment cost is higher, which is not conducive to practical applications. Therefore, it is necessary to comprehensively consider the actual requirements of investment cost and vibration suppression when selecting the mass ratio μ in vibration control.

Table 2 presents the optimal structural parameters of frequency ratio and damping ratio for different mass ratios ranging from 0.07 to 0.21. To derive more practical empirical formulas, curve fitting methods (Guest and Guest, 2012) are employed to establish the relationships between the optimal frequency ratio, optimal damping ratio, and mass ratio. These relationships are expressed in Eq. (22).

$$
\begin{cases}
\gamma_1^{opt} = 0.2826e^{0.06323\mu} + 0.0004197e^{9.834\mu}, \zeta_1^{opt} = 19.82\mu^3 - 8.436\mu^2 + 1.364\mu - 0.01739 \\
\gamma_2^{opt} = -1.385 \times 10^{-8}e^{54.97\mu} + 0.2905e^{0.5202\mu}, \quad \zeta_2^{opt} = 32.29\mu^3 - 14.409\mu^2 + 2.132\mu - 0.0473 \\
\gamma_3^{opt} = -9.401 \times 10^{-11}e^{82.98\mu} + 0.3015e^{0.8785\mu}, \quad \zeta_3^{opt} = 20.99\mu^3 - 9.702\mu^2 + 1.614\mu - 0.0293
\end{cases}
\tag{22}
$$

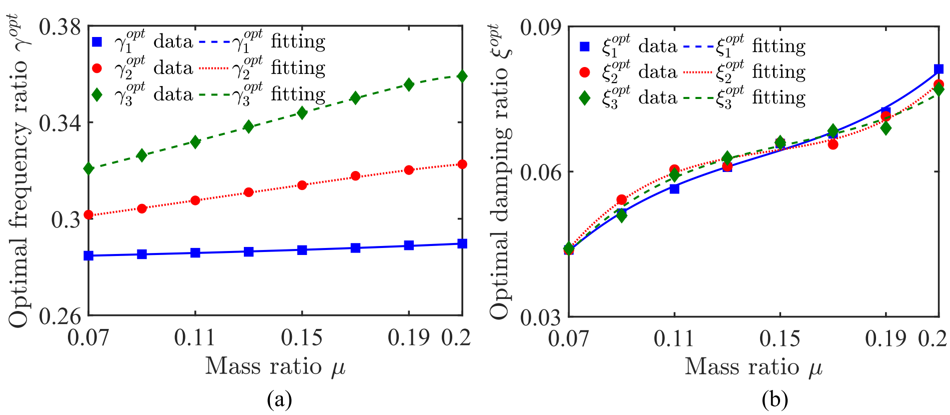

Fig. 15. Optimal parameters design of SSP-SRWEC: (a) frequency ratio, (b) damping ratio.

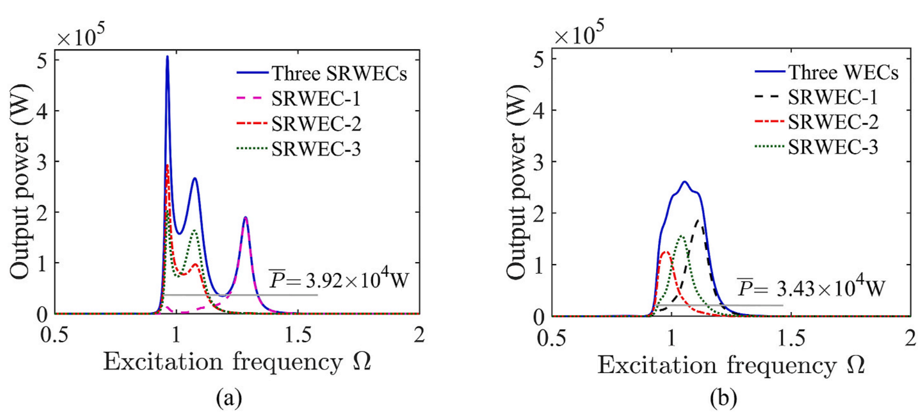

Fig. 16. Output power of SSP-SRWEC in $\mu = 0.07$: (a) under optimal energy harvesting parameters, (b) under optimal vibration control parameters.

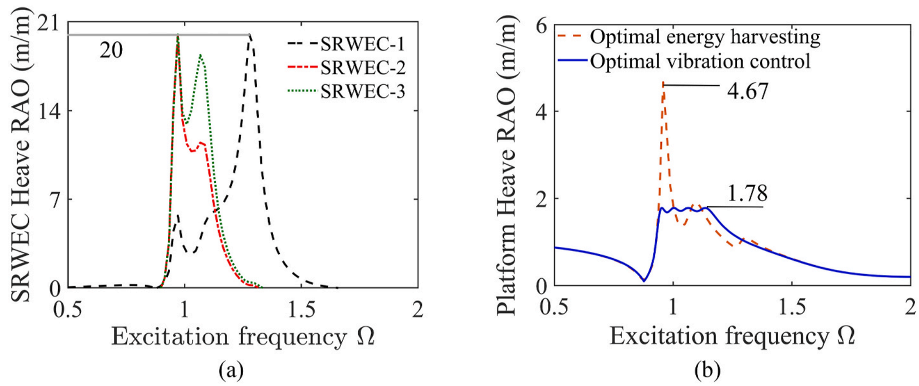

Fig. 17. The response amplitude operator of SSP-SRWEC in $\mu = 0.07$: (a) SRWEC and (b) SSP.

Table 3
Optimal frequency ratio and damping ratio under different mass ratio for energy harvesting.

Mass ratio	γ_1	ξ_1	γ_2	ξ_2	γ_3	ξ_3
μ=0.07	0.32827 ↔	0.11258 ↔	0.38771 ↔	0.01867 ↔	0.32119 ↔	0.08701 ↔
μ=0.09	0.34354 ▲	0.08095 ▼	0.44034 ▲	0.02186 ▲	0.38239 ▲	0.02819 ▼
μ=0.11	0.39113 ▲	0.09337 ▲	0.51055 ▲	0.02063 ▼	0.46929 ▲	0.02122 ▼
μ=0.13	0.42847 ▲	0.10656 ▲	0.55013 ▲	0.02294 ▲	0.49791 ▲	0.02380 ▲
μ=0.15	0.45292 ▲	0.06189 ▼	0.58962 ▲	0.02600 ▲	0.52774 ▲	0.02614 ▲
μ=0.17	0.49165 ▲	0.07351 ▲	0.63587 ▲	0.03032 ▲	0.57409 ▲	0.02467 ▼
μ=0.19	0.53576 ▲	0.08542 ▲	0.67521 ▲	0.03564 ▲	0.60658 ▲	0.02539 ▲
μ=0.21	0.53707 ▲	0.04169 ▼	0.69527 ▲	0.03894 ▲	0.61371 ▲	0.02903 ▲

It is observed from Fig. 15, the empirical formulas (Eq. (22)) exhibit a favorable fitting with the data points illustrated in Table 2, which can offer an optimal design reference for vibration control. Similar to traditional multiple dynamic vibration absorbers, when the mass ratio μ increases, the damping ratio ξ must be increased to maintain the optimal results. However, as the mass ratio μ increases, the optimal frequency ratio γ is still positively correlated with the increasing mass ratio. Because, for an SSP-SRWEC operating in the ocean, there exists added mass that varies with frequency, and its magnitude far exceeds the actual physical mass (see Fig. A1 in Appendix A1).

4.3. Energy harvesting oriented optimization

This section focuses on optimizing the energy harvesting performance of SSP-SRWEC. Optimization analysis has been performed for the excitation frequency $\Omega \in [0.5\ ,\ 2]$, which covers the most wave frequencies. Mass ratio μ is fixed as 0.07. In Fig. 16(a), under the optimal energy harvesting parameters, the power peaks of each SRWEC are scattered, occurring at 0.963, 1.075, and 1.289 resulting in three power peaks for SSP-SRWEC energy harvesting. Among these, the maximum peak output power reaches 506 kW. In contrast, under the optimal vibration control parameters, the power peaks of each SRWEC are closer, occurring at 0.978, 1.02, and 1.09. The overall output power approximates a parabola, with only one power peak, reaching 261 kW (See Fig. 16(b)). The aforementioned results demonstrate that through energy harvesting optimization, SSP-SRWEC can generate more electrical energy across a wider frequency band compared to vibration control-oriented optimization.

Interestingly, the mean power under the optimal energy harvesting parameters is only about 4.9 kW higher than the mean power under the optimal vibration control parameters. The reason is, the peak amplitude of each SRWEC can only reach a maximum of 20 m under optimal energy harvesting parameters due to the maximum motion limitation (See Fig. 17(a)). Compared with the peak amplitude of 17.8 m of SRWEC under optimal vibration control parameters, the remaining 2.2 m of optimization space can only result in a slight increase in output power.

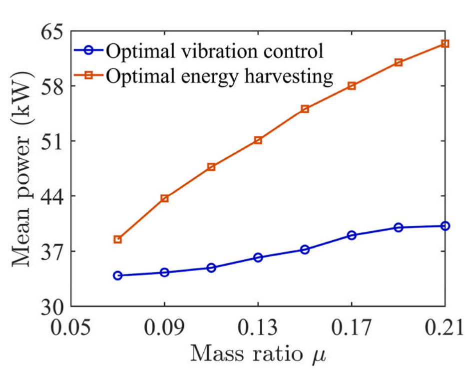

Fig. 18. The SSP-SRWEC mean power (within $\Omega \in [0.5\ ,\ 2]$) under different mass ratio μ.

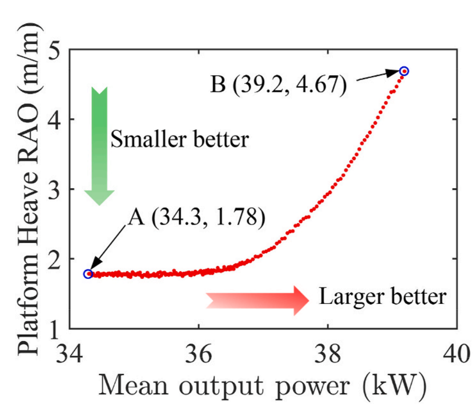

Fig. 19. Obtained Pareto front of dual-objective optimization for SSP-SRWEC.

Nevertheless, the peak amplitude of platform under the optimal energy harvesting parameters is nearly 3.38 times higher than that under the optimal vibration control parameters. The above results show that improving the output power level of SSP-SRWEC through the optimal energy harvesting method could damage the platform's reliability.

Similar to vibration control, the mass ratio will vary during the practical operation of SSP. Table 3 provides the optimal structural parameters for energy harvesting under different mass ratios. To intuitively depict the changing pattern of each optimal structural parameter with mass ratio μ in Table 3, the symbols red upper triangle ▲ and green lower triangle ▼ indicate whether the current data increases or decreases in comparison to the preceding data. The optimal structural parameters corresponding to $\mu = 0.07$ are all initial references, indicated by a double-headed arrow ⟷. It is observed from Table 3 that the frequency ratios γ_1, γ_2 and γ_3 increase as the mass ratio increases. However, the damping ratio ξ exhibits irregular change with increasing mass ratio. This irregularity can be attributed to the fact that, there is a certain practical limitation to an excursion of SRWEC in energy harvesting optimization.

Based on the above optimization parameters, the impact of mass ratio on the energy harvesting performance of SSP-SRWEC is comparatively analyzed under the optimal energy harvesting parameters and optimal vibration control parameters. As shown in Fig. 18, the mean output power of SSP-SRWEC is positively correlated with the mass ratio μ under the parameters of optimal vibration control and optimal energy harvesting. Although the increase rate is notably higher under optimal energy control parameters, the magnitude of growth remains small. For instance, at $\mu = 0.21$, the SSP-SRWEC's mean power only increases by 23.1 kW compared to $\mu = 0.07$ through energy harvesting optimization. Given that the manufacturing cost of WEC equipment is high and proportional to its mass (Chang et al., 2018; Zhang et al., 2021), compared with power improvement with smaller benefits, WEC with a smaller mass should be given priority on the basis of meeting the vibration reduction needs.

4.4. Dual-objective oriented optimization

To obtain the Pareto front, we use the PSO algorithm to perform the dual-objective optimization based on the optimization method illustrated in Fig. 12. It should be noted that, in order to reduce the construction cost of deploying SRWEC, a relatively smaller mass ratio of $\mu = 0.07$ is selected for analysis based on the results from Sections 4.2 and 4.3.

Fig. 19 presents the Pareto front of dual-objective optimization for SSP-SRWEC. It can be observed from Fig. 19 that as mean output power increases, the platform response amplitude operator (RAO) also increases. However, for vibration control, smaller vibration amplitude is better, while the opposite is true for energy harvesting. This implies a conflict between maximizing power output and minimizing platform motion. In the above Pareto front, the leftmost point A (34.3, 1.78) represents a solution with a lowest platform heave RAO and lowest mean output power, whereas the rightmost point B (39.2, 4.67) represents a solution with the highest mean output power and the highest platform heave RAO. From extreme point A to point B, although the average output power can be increased by about 5 kW, the platform vibration response increases sharply by 163%. Given the very high construction and maintenance costs of offshore floating platform, vibration control performance should be a top priority in dual-objective optimization.

As a summary of this section, it should be noted that.

(1) Through energy harvesting optimization, SSP-SRWEC can generate more electrical energy across a wider frequency band compared to vibration control-oriented optimization. However, this increase in output power comes at the expense of platform stability. (2) Increasing the mass of SRWEC can decrease SSP vibration amplitude, but an excessive mass ratio μ means high WEC investment costs. Moreover, given the limited power increase from mass increment, WEC with a smaller mass should be

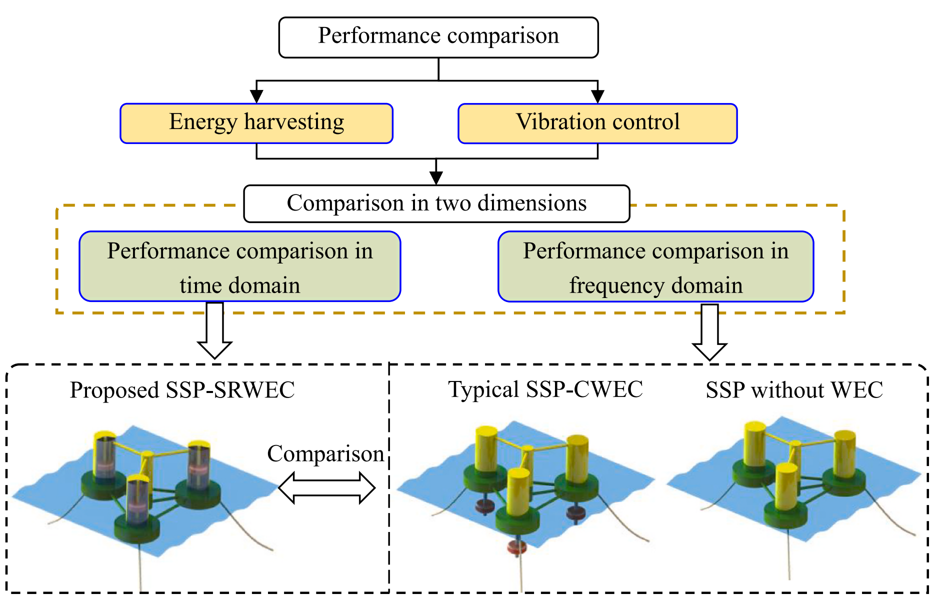

Fig. 20. Framework of performance comparison of the proposed SSP-SRWEC.

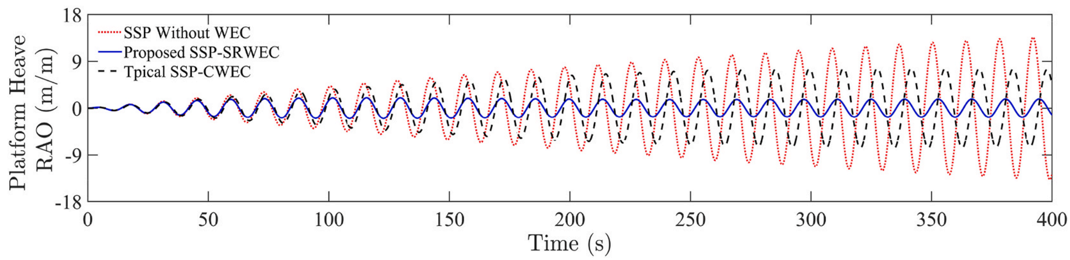

Fig. 21. The platform vibration of the SSP-SRWEC, SSP-CWEC and SSP without WEC.

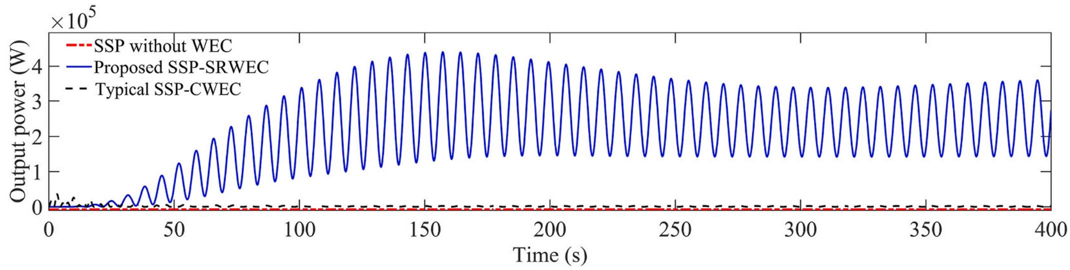

Fig. 22. The output power of the SSP-SRWEC and SSP-CWEC and SSP without WEC.

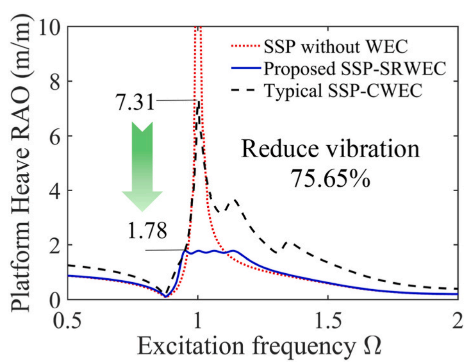

Fig. 23. The Response amplitude operator of SSP-SRWEC the SSP-SRWEC, SSP-CWEC and SSP without WEC under different excitation frequency (in the range of [0.5, 2]).

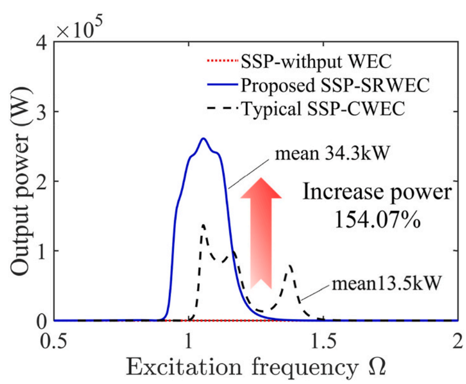

Fig. 24. The output power of SSP-SRWEC the SSP-SRWEC, SSP-CWEC and SSP without WEC under different excitation frequency (in the range of [0.5, 2]).

given priority on the basis of meeting the vibration reduction needs.

(3) In dual-objective optimization, prioritizing energy harvesting only slightly raises power output but significantly increases platform vibration at resonance, posing risks to the SSP. Given the high cost of offshore SSP, vibration control performance should be a top priority in dual-objective optimization.

5. Performance comparison

To demonstrate the overall vibration control and energy harvesting performances of the proposed SSP-SRWECs, as shown in Fig. 20, we conduct a performance comparison of the proposed SSP-SRWEC, typical SSP-CWEC, and SSP without WEC. To be specific, the comparison in two dimensions includes (i) Performance comparison in the time domain, (ii) Performance comparison in the frequency domain.

For the fairness of comparison, the structural parameters of SSP, the number, mass and operation mechanism of each WECs are the same for the SSP-SRWEC and SSP-CWEC. The motion equations for the SSP-CWEC are adopted from those widely derived in the literature (Dhanak and Xiros, 2016; Ghafari et al., 2021; Hu et al., 2020; Zhou et al., 2023), and the derivation process shall not be repeated here. Its model is shown in Appendix A2 for brevity. Moreover, considering the importance of the safe operation of the floating platform, considering the importance of the safe operation of the floating platform, we have unified our optimization objective to focus solely on vibration control (see Eq. (17)) for both the SSP-SRWEC and the SSP-CWEC. According to the optimization method in Section 4.1, the optimal stiffness values of the WECs in the SSP-CWEC are obtained as 21.8 kN/m, 34.5 kN/m, and 24.3 kN/m, while the corresponding optimal damping parameters are 5.57 kNs/m, 2.66 kNs/m, and 3.97 kNs/m, respectively. Other system structural parameters are adopted from Table 1.

5.1. Performance comparison in time domain

Fig. 21 presents the platform vibration of the proposed SSP-SRWEC, typical SSP-CWEC and SSP without WEC in wave height $H = 2$ m and $\Omega = 0.994$ ("National Science & Technology Infrastructure. Measured Data. Available at: http://mds.nmdis.org.cn). In comparison, the SSP-SRWEC has excellent vibration control performance. Specifically, the platform vibration amplitudes in steady state are 1.78 m, 7.1 m and 13.6 m for SSP-SRWEC, SSP-CWEC and SSP without WEC, respectively. The SSP-SRWEC reduces vibration amplitude by approximately 74.9% and 86.9% more than SSP-CWEC and SSP without WEC, respectively. Moreover, Fig. 22 shows that the SSP-SRWEC has a much greater output power than the SSP-CWEC and SSP without WEC. Note that the output power of SSP without WEC is zero because it does not contain power generation equipment. This substantial difference in energy harvesting can be used to explain why SSP-SRWEC has the lowest vibration amplitude.

5.2. Performance comparison in frequency domain

The wave excitation frequency will change due to the influence of external factors, thus impacting SSP-SRWEC's performance in energy harvesting and vibration control. In view of this, performance comparison analysis is performed for the excitation frequency $\Omega \in [0.5\ ,\ 2]$, which covers the most wave frequency. As shown in Figs. 23 and 24, the proposed SSP-SRWEC exhibits superior performance in both vibration control and energy harvesting compared to the typical SSP-CWEC, resulting in an 75.65% reduction in the SSP's resonant peak and a 154.07% increase in WEC's energy harvesting. More importantly, the SSP-SRWEC has widened vibration suppression bandwidth across different wave frequencies, which provides good robustness in practice engineering.

6. Conclusions

Combining the multiple wave energy converters (WECs) into the offshore floating platform (OFP) is a conventional way to suppress vibration and harvest wave energy. However, the WECs are all installed outside of the OFP, leading to interactions among the WECs, OFP, and wave hydrodynamics. It means that the WECs may not effectively reduce OFP vibration amplitude by directly absorbing platform vibration energy. To solve this issue, using the most widely used semi-submersible floating platform (SSP) as an example, a novel SSP synergizing multiple internally-installed self-reacting WECs (SSP-SRWEC) is proposed in this study. Subsequently, the dynamic model of SSP-SRWEC is established and verified. Based on the model, the optimization analysis and performance comparison are performed. The following conclusion can be drawn:

(1) Increasing the mass of SRWEC can decrease SSP vibration amplitude, but an excessive mass ratio μ means high WEC investment costs. Also, given the limited power increase from mass increment, WEC with a smaller mass should be given priority on the basis of meeting the vibration reduction needs.

(2) As mass ratio μ rises, optimal vibration control requires increasing both damping ratio ξ and frequency ratio γ. Similarly, to maintain optimal energy harvesting, frequency ratio γ must be raised with increasing μ. However, the optimal damping ratio ξ of energy harvesting exhibits fluctuate irregularly due to practical motion constraints on SRWEC.

(3) In dual-objective oriented optimization, prioritizing energy harvesting will only increase output power slightly, meanwhile, the vibration amplitude of the platform at the resonant frequency will increase significantly. To ensure the safe operation of high-cost OFP, vibration control performance should be top-prioritized in dual-objective optimization.

(4) By internally installing the multiple WECs with self-reacting mechanism into the floating platform, compared to the typical SSP-CWEC, the proposed SSP-SRWEC effectively suppresses the SSP resonance peak by 75.65% and increases WEC's energy harvesting by 154.07%. Additionally, it significantly widens the vibration suppression bandwidth, making it highly desirable in practice.

In summary, this paper makes a modest contribution by extending the operation mechanism of internally installed WEC into the floating platform vibration control scenario and conducting a numerical optimization investigation. Results show that the proposed SSP-SRWEC demonstrates superior performance in both vibration control and energy harvesting under varying external wave frequencies. However, this analysis effort is only the first step toward making the proposed idea a practical application. The use of more advanced PTO controller structures for vibration control lacks sufficient research. We plan to investigate improvements to the PTO controller structure in future work.

CRediT authorship contribution statement

Zhicong Huang: Writing – original draft, Resources, Project administration, Investigation, Funding acquisition, Conceptualization. **Yongxing Zhang:** Writing – original draft, Conceptualization. **Jing Bian:** Writing – review & editing, Visualization, Supervision, Conceptualization.

Declaration of competing interest

The authors declare that they have no known competing financial interests or personal relationships that could have appeared to influence the work reported in this paper.

Acknowledgments

This work was supported by the Science and Technology Planning Project of Guangdong Province under (Grant No. 2023A0505050124), the Science and Technology Project of China Southern Power Grid, (Grant No. 0300002023030103GH00130), the National Natural Science Foundation of China (Grant Nos. 52007067, 52308144) and China Postdoctoral Science Foundation (Grant No. 2022M720576).

Appendix A1. Hydrodynamic parameters of SSP-SRWEC

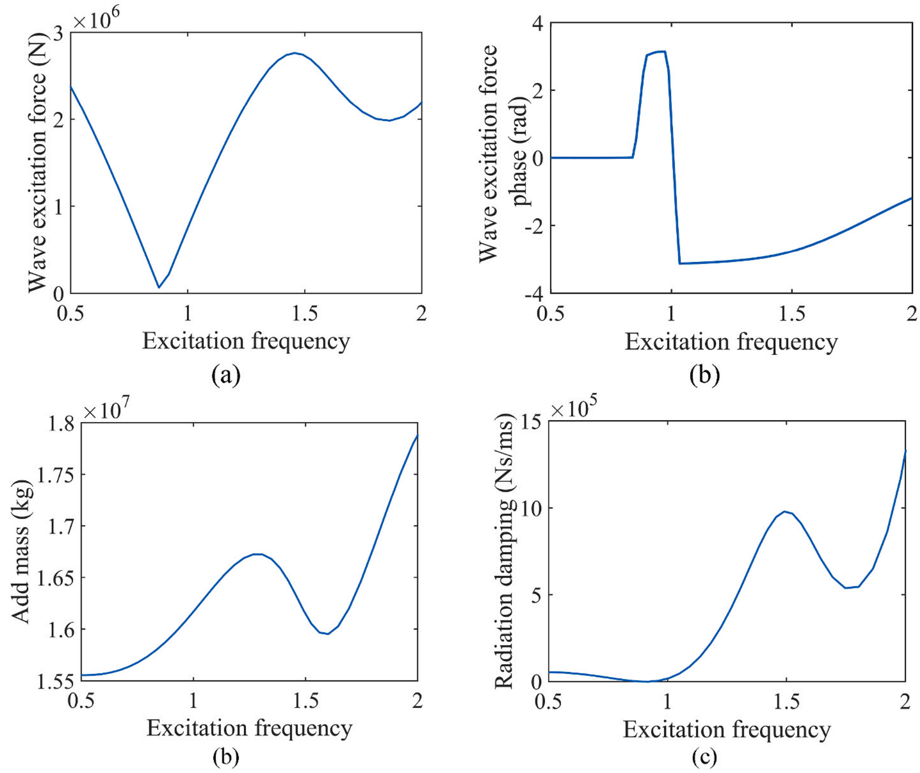

Fig. A1. Hydrodynamic parameters of SSP-SRWEC in the heave direction: (a) wave excitation force, (b) wave excitation force phase, (c) added mass and (d) radiation damping.

Appendix A2. The model of SSP-CWEC in frequency domain

$$\left\{-\omega^2\left[m_p+m_{add}(\omega)\right]+k_p+j\omega c_p(\omega)\right\}Z_p(j\omega)-\sum_{i=1}^{3}\left\{\left[Z_{wi}(j\omega)-Z_p(j\omega)\right](k_{wi}+j\omega c_{wi})\right\}=F_e(j\omega) \quad \text{(A. 1)}$$

$$\left\{-\omega^2\left[m_w+m_{c,add}(\omega)\right]+k_{c,w}+j\omega c_{c,w}(\omega)\right\}Z_{wi}(j\omega)+(k_{wi}+j\omega c_{wi})\left[Z_{wi}(j\omega)-Z_p(j\omega)\right]=F_{c,e}(j\omega) \quad \text{(A. 2)}$$

where $F_{c,e}(j\omega)$ is the wave excitation forces acting on the WEC in the frequency domain. $m_{c,add}$ (ω), $c_{c,w}$ (ω) and $k_{c,w}$ represent the frequency-dependent added mass, frequency-dependent radiation damping, and hydrostatic stiffness for the WEC.

References

Albert, A., Berselli, G., Bruzzone, L., Fanghella, P., 2017. Mechanical design and simulation of an onshore four-bar wave energy converter. Renew. Energy 114, 766–774.

Babarit, A., Delhommeau, G., 2015. Theoretical and numerical aspects of the open source BEM solver NEMOH. In: 11th European Wave and Tidal Energy Conference (EWTEC2015).

Bao, X., Li, F., Sun, H., Iglesias, G., Shi, H., 2023. Performance characteristics and parameter analysis of a multi-DOF wave energy converter with hybrid power take-off systems. Energy Convers. Manag. 278, 116751.

Bian, J., 2021. Analysis and Design of Nonlinear Damping and its Application. The Hoog Kong Polytechnic university. PhD thesis.

Bian, J., Jing, X., 2021. A nonlinear X-shaped structure based tuned mass damper with multi-variable optimization (X-absorber). Commun. Nonlinear Sci. Numer. Simul. 99, 105829.

Bian, J., Jing, X., 2020. Analysis and design of a novel and compact X-structured vibration isolation mount (X-Mount) with wider quasi-zero-stiffness range. Nonlinear Dynam. 101, 2195–2222. https://doi.org/10.1007/s11071-020-05878-y.

Bian, J., Zhou, X., Ke, K., Yam, M.C., Wang, Y., 2022. Seismic resilient steel substation with BI-TMDI: a theoretical model for optimal design. J. Constr. Steel Res. 192, 107233.

Bian, J., Zhou, X., Ke, K., Yam, M.C., Wang, Y., Qiu, Y., 2023. A passive vibration isolator with bio-inspired structure and inerter nonlinear effects. Struct. Eng. Mech. 88, 221.

Blum, E.K., 1962. A modification of the Runge-Kutta fourth-order method. Math. Comput. 16, 176–187.

Bracco, G., Canale, M., Cerone, V., 2020. Optimizing energy production of an inertial sea wave energy converter via model predictive control. Control Eng. Pract. 96, 104299.

Bruzzone, L., Fanghella, P., Berselli, G., 2020. Reinforcement learning control of an onshore oscillating arm wave energy converter. Ocean Eng. 206, 107346.

Calinescu, R., Češka, M., Gerasimou, S., Kwiatkowska, M., Paoletti, N., 2018. Efficient synthesis of robust models for stochastic systems. J. Syst. Software 143, 140–158. https://doi.org/10.1016/j.jss.2018.05.013.

Carapellese, F., Pasta, E., Faedo, N., Giorgi, G., 2022a. Dynamic analysis and performance assessment of the Inertial Sea Wave Energy Converter (ISWEC) device via harmonic balance. IFAC-PapersOnLine 55, 439–444.

Carapellese, F., Pasta, E., Paduano, B., Faedo, N., Mattiazzo, G., 2022b. Intuitive LTI energy-maximising control for multi-degree of freedom wave energy converters: the PeWEC case. Ocean Eng. 256, 111444.

Chai, Y., Bian, J., Li, M., 2024. A novel quasi-zero-stiffness isolation platform via tunable positive and negative stiffness compensation mechanism. Nonlinear Dynam. 112, 101–123. https://doi.org/10.1007/s11071-023-09018-0.

Chang, G., Jones, C.A., Roberts, J.D., Neary, V.S., 2018. A comprehensive evaluation of factors affecting the levelized cost of wave energy conversion projects. Renew. Energy 127, 344–354.

Chen, T., Li, M., Yao, X., 2019. Standing on the shoulders of giants: seeding search-based multi-objective optimization with prior knowledge for software service composition. Inf. Software Technol. 114, 155–175. https://doi.org/10.1016/j.infsof.2019.05.013.

Cheng, Y., Fu, L., Dai, S., Collu, M., Cui, L., Yuan, Z., Incecik, A., 2022a. Experimental and numerical analysis of a hybrid WEC-breakwater system combining an oscillating water column and an oscillating buoy. Renew. Sustain. Energy Rev. 169, 112909.

Cheng, Y., Fu, L., Dai, S., Collu, M., Ji, C., Yuan, Z., Incecik, A., 2022b. Experimental and numerical investigation of WEC-type floating breakwaters: a single-pontoon

oscillating buoy and a dual-pontoon oscillating water column. Coast. Eng. 177, 104188.
Cheng, Y., Gong, J., Zhang, J., 2024. Hydrodynamic investigation on a single-point moored offshore cage-wave energy converter hybrid system. Ocean Eng. 299, 116848.
Cummins, W., 1962. The impulse response function and ship motions. Schiffstechnik 9, 101–109.
Dhanak, M.R., Xiros, N.I., 2016. Springer Handbook of Ocean Engineering. Springer.
Emami, A., Gharabaghi, A.R.M., 2020. Application of poroelastic layers in a semi-submersible platform: devising an efficient heave motion response reduction method. Ocean Eng. 201, 107148.
Esmaeilzadeh, S., Alam, M.-R., 2019. Shape optimization of wave energy converters for broadband directional incident waves. Ocean Eng. 174, 186–200. https://doi.org/10.1016/j.oceaneng.2019.01.029.
Falcão, A.F., Henriques, J.C., Gato, L.M., 2018. Self-rectifying air turbines for wave energy conversion: a comparative analysis. Renew. Sustain. Energy Rev. 91, 1231–1241.
Farahpour, H., Hejazi, F., 2023. Development of integrated semi-active adaptive vibration control system for bridges subjected to traffic loads. In: Structures. Elsevier, pp. 1773–1794.
Gaspar, J.F., Hallak, T.S., Soares, C.G., 2018. Semi-submersible platform concept for a concentric array of wave energy converters. In: Advances in Renewable Energies Offshore: Proceedings of the 3rd International Conference on Renewable Energies Offshore (RENEW 2018), October 8-10, 2018. CRC Press, Lisbon, Portugal, p. 307.
Gaspar, J.F., Kamarlouei, M., Thiebaut, F., Soares, C.G., 2021. Compensation of a hybrid platform dynamics using wave energy converters in different sea state conditions. Renew. Energy 177, 871–883.
Ghafari, H.R., Ghassemi, H., He, G., 2021. Numerical study of the Wavestar wave energy converter with multi-point-absorber around DeepCwind semisubmersible floating platform. Ocean Eng. 232, 109177.
Guest, P.G., Guest, P.G., 2012. Numerical Methods of Curve Fitting. Cambridge University Press.
Halkyard, J., 2005. Floating offshore platform design. In: Handbook of Offshore Engineering. Elsevier, pp. 419–661.
Hemmati, A., Oterkus, E., Khorasanchi, M., 2019. Vibration suppression of offshore wind turbine foundations using tuned liquid column dampers and tuned mass dampers. Ocean Eng. 172, 286–295.
Hu, J., Zhou, B., Vogel, C., Liu, P., Willden, R., Sun, K., Zang, J., Geng, J., Jin, P., Cui, L., 2020. Optimal design and performance analysis of a hybrid system combing a floating wind platform and wave energy converters. Appl. Energy 269, 114998.
Huang, X., Yang, B., 2023. Towards novel energy shunt inspired vibration suppression techniques: principles, designs and applications. Mech. Syst. Signal Process. 182, 109496.
Huang, Y., Lan, H., Hong, Y.-Y., Wen, S., Yin, H., 2019. Optimal generation scheduling for a deep-water semi-submersible drilling platform with uncertain renewable power generation and loads. Energy 181, 897–907.
Kamarlouei, M., Gaspar, J.F., Calvario, M., Hallak, T.S., Mendes, M.J., Thiebaut, F., Soares, C.G., 2020. Experimental analysis of wave energy converters concentrically attached on a floating offshore platform. Renew. Energy 152, 1171–1185.
Kandasamy, R., Cui, F., Townsend, N., Foo, C.C., Guo, J., Shenoi, A., Xiong, Y., 2016. A review of vibration control methods for marine offshore structures. Ocean Eng. 127, 279–297.
Ke, K., Bian, J., Zhou, X.-H., Yam, M.C., Wang, Y.-H., Gu, Z., Sun, M., 2023. A novel prismatic-shaped isolation platform with tunable negative stiffness and enhanced quasi-zero stiffness effect. Smart Struct. Syst. Int. J. 31, 213–227.
Khedkar, K., Nangia, N., Thirumalaisamy, R., Bhalla, A.P.S., 2021. The inertial sea wave energy converter (ISWEC) technology: device-physics, multiphase modeling and simulations. Ocean Eng. 229, 108879.
Kim, D., Song, S., Jeong, B., Tezdogan, T., Incecik, A., 2021a. Unsteady RANS CFD simulations of ship manoeuvrability and course keeping control under various wave height conditions. Appl. Ocean Res. 117, 102940.
Kim, D., Song, S., Tezdogan, T., 2021b. Free running CFD simulations to investigate ship manoeuvrability in waves. Ocean Eng. 236, 109567.
Lamas-Pardo, M., Iglesias, G., Carral, L., 2015. A review of very large floating structures (VLFS) for coastal and offshore uses. Ocean Eng. 109, 677–690.
Liu, Y., Li, S., Yi, Q., Chen, D., 2016. Developments in semi-submersible floating foundations supporting wind turbines: a comprehensive review. Renew. Sustain. Energy Rev. 60, 433–449.
Ma, R., Bi, K., Hao, H., 2021. Wave flume tests of a semi-submersible platform controlled by a novel rotational inertia damper. Ocean Eng. 238, 109718.
Ma, R., Bi, K., Hao, H., 2020. Heave motion mitigation of semi-submersible platform using inerter-based vibration isolation system (IVIS). Eng. Struct. 219, 110833.
Ma, R., Bi, K., Hao, H., 2019. A novel rotational inertia damper for heave motion suppression of semisubmersible platform in the shallow sea. Struct. Control Health Monit. 26. https://doi.org/10.1002/stc.2368.
Ma, R., Bi, K., Zuo, H., Du, X., 2023. Inerter-based damping isolation system for vibration control of offshore platforms subjected to ground motions. Ocean Eng. 280, 114726.
Marini, F., Walczak, B., 2015. Particle swarm optimization (PSO). A tutorial. Chemometr. Intell. Lab. Syst. 149, 153–165.
Muliawan, M.J., Karimirad, M., Moan, T., 2013. Dynamic response and power performance of a combined spar-type floating wind turbine and coaxial floating wave energy converter. Renew. Energy 50, 47–57.
National Science & Technology Infrastructure. Measured Data. Available at: http://mds.nmdis.org.cn.
Nguyen, H.P., Wang, C.M., 2020a. Oscillating wave surge converter-type attachment for extracting wave energy while reducing hydroelastic responses of very large floating structures. J. Offshore Mech. Arctic Eng. 142, 042001.
Nguyen, H.P., Wang, C.M., 2020b. Heaving wave energy converter-type attachments to a pontoon-type very large floating structure. Eng. Struct. 219, 110964.
Oliveira-Pinto, S., Rosa-Santos, P., Taveira-Pinto, F., 2019. Electricity supply to offshore oil and gas platforms from renewable ocean wave energy: overview and case study analysis. Energy Convers. Manag. 186, 556–569.
Pata, U.K., 2021. Renewable and non-renewable energy consumption, economic complexity, CO2 emissions, and ecological footprint in the USA: testing the EKC hypothesis with a structural break. Environ. Sci. Pollut. Res. 28, 846–861. https://doi.org/10.1007/s11356-020-10446-3.
Pozzi, N., Bracco, G., Passione, B., Sirigu, S.A., Mattiazzo, G., 2018. PeWEC: experimental validation of wave to PTO numerical model. Ocean Eng. 167, 114–129.
Rehman, S., Alhems, L.M., Alam, M.M., Wang, L., Toor, Z., 2023. A review of energy extraction from wind and ocean: technologies, merits, efficiencies, and cost. Ocean Eng. 267, 113192.
Rodríguez, C.A., Rosa-Santos, P., Taveira-Pinto, F., 2020. Hydrodynamic optimization of the geometry of a sloped-motion wave energy converter. Ocean Eng. 199, 107046. https://doi.org/10.1016/j.oceaneng.2020.107046.
Rodríguez, C.A., Rosa-Santos, P., Taveira-Pinto, F., 2019. Assessment of damping coefficients of power take-off systems of wave energy converters: a hybrid approach. Energy 169, 1022–1038. https://doi.org/10.1016/j.energy.2018.12.081.
Rony, J.S., Karmakar, D., 2022. Coupled dynamic analysis of hybrid offshore wind turbine and wave energy converter. J. Offshore Mech. Arctic Eng. 144, 032002.
Ropero-Giralda, P., Crespo, A.J.C., Coe, R.G., Tagliafierro, B., Domínguez, J.M., Bacelli, G., Gómez-Gesteira, M., 2021. Modelling a heaving point-absorber with a closed-loop control system using the DualSPHysics code. Energies 14, 760. https://doi.org/10.3390/en14030760.
Saeed, N., Gong, J., Wan, Y., Long, K., Saeed, A., Mei, L., Xiong, C., Long, W., Zhou, H., Li, L., 2024. A novel design of multifunctional offshore floating platform structure based on topology optimization. Eng. Struct. 306, 117782.
Sebastian, B., Karmakar, D., Rao, M., 2024. Coupled dynamic analysis of semi-submersible floating wind turbine integrated with oscillating water column WEC. J. Ocean Eng. Mar. Energy 10, 287–312. https://doi.org/10.1007/s40722-023-00313-x.
Shadman, M., Estefen, S.F., Rodriguez, C.A., Nogueira, I.C.M., 2018. A geometrical optimization method applied to a heaving point absorber wave energy converter. Renew. Energy 115, 533–546. https://doi.org/10.1016/j.renene.2017.08.055.
Sharma, R., Kim, T.-W., Sha, O.P., Misra, S.C., 2010. Issues in offshore platform research-Part 1: semi-submersibles. Int. J. Nav. Archit. Ocean Eng. 2, 155–170.
Shi, J., Zhang, H., Huang, X., Wen, J., Chen, Guoming, Chen, Guoxin, Yu, A., 2024. Experimental and numerical study of gas explosion from semi-submersible platform. Ocean Eng. 295, 116958.
Su, N., Bian, J., Peng, S., Chen, Z., Xia, Y., 2023. Balancing static and dynamic performances of TMD with negative stiffness. Int. J. Mech. Sci. 243, 108068.
Su, N., Chen, Z., Xia, Y., Bian, J., 2024. Hybrid analytical H-norm optimization approach for dynamic vibration absorbers. Int. J. Mech. Sci. 264, 108796.
Sykes, V., Collu, M., Coraddu, A., 2023. A review and analysis of optimisation techniques applied to floating offshore wind platforms. Ocean Eng. 285, 115247. https://doi.org/10.1016/j.oceaneng.2023.115247.
Taghipour, R., Perez, T., Moan, T., 2008. Hybrid frequency–time domain models for dynamic response analysis of marine structures. Ocean Eng. 35, 685–705. https://doi.org/10.1016/j.oceaneng.2007.11.002.
Tao, J., Cao, F., Dong, X., Li, D., Shi, H., 2021. Optimized design of 3-DOF buoy wave energy converters under a specified wave energy spectrum. Appl. Ocean Res. 116, 102885.
Terziev, M., Tezdogan, T., Incecik, A., 2022. Scale effects and full-scale ship hydrodynamics: a review. Ocean Eng. 245, 110496.
Terziev, M., Tezdogan, T., Incecik, A., 2021. Modelling the hydrodynamic effect of abrupt water depth changes on a ship travelling in restricted waters using CFD. Ships Offshore Struct. 16, 1087–1103. https://doi.org/10.1080/17445302.2020.1816731.
Terziev, M., Tezdogan, T., Incecik, A., 2020. Application of eddy-viscosity turbulence models to problems in ship hydrodynamics. Ships Offshore Struct. 15, 511–534. https://doi.org/10.1080/17445302.2019.1661625.
Tezdogan, T., Demirel, Y.K., Kellett, P., Khorasanchi, M., Incecik, A., Turan, O., 2015. Full-scale unsteady RANS CFD simulations of ship behaviour and performance in head seas due to slow steaming. Ocean Eng. 97, 186–206.
Tezdogan, T., Incecik, A., Turan, O., 2016a. A numerical investigation of the squat and resistance of ships advancing through a canal using CFD. J. Mar. Sci. Technol. 21, 86–101. https://doi.org/10.1007/s00773-015-0334-1.
Tezdogan, T., Incecik, A., Turan, O., 2016b. Full-scale unsteady RANS simulations of vertical ship motions in shallow water. Ocean Eng. 123, 131–145.
Tian, W., Wang, Y., Shi, W., Michailides, C., Wan, L., Chen, M., 2023. Numerical study of hydrodynamic responses for a combined concept of semisubmersible wind turbine and different layouts of a wave energy converter. Ocean Eng. 272, 113824.
Vervaet, T., Stratigaki, V., Ferri, F., De Beule, L., Claerbout, H., De Witte, B., Vantorre, M., Troch, P., 2022. Experimental modelling of an isolated wecfarm real-time controllable heaving point absorber wave energy converter. J. Mar. Sci. Eng. 10, 1480.
Wang, Y., Shi, W., Michailides, C., Wan, L., Kim, H., Li, X., 2022. WEC shape effect on the motion response and power performance of a combined wind-wave energy converter. Ocean Eng. 250, 111038.
Wei, Z., Shi, H., Cao, F., Yu, M., Li, M., Chen, Z., Liu, P., 2024. Study on the power performance of wave energy converters mounted around an offshore wind turbine jacket platform. Renew. Energy 221, 119786.

Wu, H., Zhu, F., Yuan, Z., 2024. Effects of the WEC shape on the performance of a novel hybrid WEC-FOWT system. Energy 288, 129907.

Yang, J., He, E.M., Hu, Y.Q., 2019. Dynamic modeling and vibration suppression for an offshore wind turbine with a tuned mass damper in floating platform. Appl. Ocean Res. 83, 21–29.

Yang, L., Huang, J., Congpuong, N., Chen, S., Mi, J., Bacelli, G., Zuo, L., 2021. Control co-design and characterization of a power takeoff for wave energy conversion based on active mechanical motion rectification. IFAC-PapersOnLine 54, 198–203.

Yao, J.T.P., 1972. Concept of structural control. J. Struct. Div. 98, 1567–1574. https://doi.org/10.1061/JSDEAG.0003280.

Yin, X., Li, X., Zuo, L., 2019. Dynamic characteristics and test results of a wave power takeoff system with mechanical motion rectification and transmission. IEEE Trans. Ind. Electron. 68, 12262–12271.

Zhang, B.-L., Han, Q.-L., Zhang, X.-M., 2017. Recent advances in vibration control of offshore platforms. Nonlinear Dynam. 89, 755–771. https://doi.org/10.1007/s11071-017-3503-4.

Zhang, D., Chen, Z., Liu, X., Sun, J., Yu, H., Zeng, W., Ying, Y., Sun, Y., Cui, L., Yang, S., 2022. A coupled numerical framework for hybrid floating offshore wind turbine and oscillating water column wave energy converters. Energy Convers. Manag. 267, 115933.

Zhang, H., Zhang, N., Cao, X., 2023. Conceptualization and dynamic response of an integrated system with a semi-submersible floating wind turbine and two types of wave energy converters. Ocean Eng. 269, 113517.

Zhang, Y., Harman, M., Ochoa, G., Ruhe, G., Brinkkemper, S., 2018. An empirical study of meta- and hyper-heuristic search for multi-objective release planning. ACM Trans. Software Eng. Methodol. 27, 1–32. https://doi.org/10.1145/3196831.

Zhang, Y., Huang, Z., Zou, B., Bian, J., 2023. Conceptual design and analysis for a novel parallel configuration-type wave energy converter. Renew. Energy 208, 627–644. https://doi.org/10.1016/j.renene.2023.03.086.

Zhang, Y., Zhao, Y., Sun, W., Li, J., 2021. Ocean wave energy converters: technical principle, device realization, and performance evaluation. Renew. Sustain. Energy Rev. 141, 110764.

Zhang, Z., Chen, X., Wu, H., Liu, W., Cui, L., 2023. Numerical study of a novel hybrid system with the Wavestar wave energy converter array and a SPIC semi-submersible floating platform. J. Clean. Prod. 407, 137178.

Zhao, Y., Yuan, H., Zhang, Z., Gao, Q., 2024. Performance analysis and multi-objective optimization of the offshore renewable energy powered integrated energy supply system. Energy Convers. Manag. 304, 118232.

Zhou, B., Hu, J., Jin, P., Sun, K., Li, Y., Ning, D., 2023. Power performance and motion response of a floating wind platform and multiple heaving wave energy converters hybrid system. Energy 265, 126314.

Zhu, H., Hu, C., 2016. A study on control of wave energy converter for motion suppression of semisubmersible. IFAC-PapersOnLine 49, 380–385.

Zou, S., Abdelkhalik, O., 2020. Collective control in arrays of wave energy converters. Renew. Energy 156, 361–369.